Void Growth and Collapse in Viscous Solids

by B. BUDIANSKY, J. W. HUTCHINSON, and S. SLUTSKY

Division of Applied Sciences, Harvard University

Summary

Deformation of an isolated void in an infinite block of linearly or nonlinearly viscous material is studied for remote axisymmetric stressing. The material is isotropic and incompressible with a power-law dependence of strain-rate on stress. Included in the family of materials are a linearly viscous solid and a rigid–perfectly plastic solid at the extreme limit of nonlinearity. Evolution of the void shape and size is analyzed in detail for voids starting as spheres in the linearly viscous material under all possible combinations of remote axisymmetric stressing. Asymptotic, or self-similar, shapes towards which the voids evolve are exhibited as are the associated rates of growth or collapse. Under conditions of high remote triaxial stressing the growth-rate of the asymptotic void is found to be identical to that of a spherical void with the same volume. The influence of nonlinearity on the growth-rate and deformation of a spherical void is investigated. Under high triaxiality conditions the behavior of a void in the nonlinearly viscous or rigid–perfectly plastic material is qualitatively different from that of a void in a linearly viscous material. In particular, a void in a nonlinear block undergoing tensile straining with sufficiently large superimposed remote hydrostatic tension grows more rapidly in directions perpendicular to the straining direction than along it and becomes significantly oblate. Asymptotic growth-rates are estimated numerically for the nonlinear materials. The results for the isolated void are used in a simple, approximate way to investigate the roles of material nonlinearity and stressing conditions on the strain required for ductile failure by void growth and coalescence.

1. Introduction

The roles of material nonlinearity and stress state on void growth or collapse in viscous solids are studied in this article. The materials considered are isotropic and incompressible with power-law dependence of strain-rate on stress. Under simple tension σ, the associated strain-rate $\dot{\varepsilon}$ is

$$\dot{\varepsilon} = \dot{\varepsilon}_0(\sigma/\sigma_0)^n \tag{1.1}$$

where $\dot{\varepsilon}_0$ and σ_0 are reference strain-rate and stress quantities. The hardening exponent n ranges from unity to infinity. For multiaxial stress states σ_{ij}, (1.1) is generalized to

13

$$\dot{\varepsilon}_{ij} = \frac{3}{2}\dot{\varepsilon}_0(\sigma_e/\sigma_0)^{n-1}s_{ij}/\sigma_0, \tag{1.2}$$

where s_{ij} is the stress deviator, $\sigma_e = (3s_{ij}s_{ij}/2)^{1/2}$ is the effective stress, and $\dot{\varepsilon}_{ij}$ is the strain-rate. For convenience, (1.2) will be used throughout in the more compact form

$$\dot{\varepsilon}_{ij} = \frac{1}{2\eta}\sigma_e^{n-1}s_{ij} \tag{1.3}$$

where η is a viscosity-like parameter defined by

$$\eta = \sigma_0^n/(3\dot{\varepsilon}_0). \tag{1.4}$$

Included in this family of materials is a linear Newtonian viscous solid with $n = 1$ and a rigid–perfectly plastic solid with $n \to \infty$. Hill (1956) singled out the family of materials (1.3) as being particularly appropriate for the investigation of a wide range of material behaviors—a viewpoint which is adopted here.

The study presented below is restricted to an investigation of the growth or collapse of an isolated void in an infinite block of material. Furthermore, the void is axisymmetric with respect to the x_3-axis and the stresses remote from the void are also axisymmetric with respect to this axis. The following notation for the nonzero remote stresses will be used throughout:

$$\sigma_{11}^\infty = \sigma_{22}^\infty = T, \qquad \sigma_{33}^\infty = S. \tag{1.5}$$

In addition, it is useful to introduce the notation

$$\sigma_m = \frac{1}{3}\sigma_{ii}^\infty = \frac{1}{3}(S + 2T) \tag{1.6}$$

for the remote mean stress, and to let

$$\sigma = S - T \tag{1.7}$$

so that $\sigma_e^\infty = |\sigma|$. The nonzero remote strain-rates are

$$\dot{\varepsilon}_{33}^\infty = -2\dot{\varepsilon}_{11}^\infty = -2\dot{\varepsilon}_{22}^\infty \equiv \dot{\varepsilon}, \tag{1.8}$$

where

$$\dot{\varepsilon} = \frac{1}{3\eta}|\sigma|^{n-1}\sigma. \tag{1.9}$$

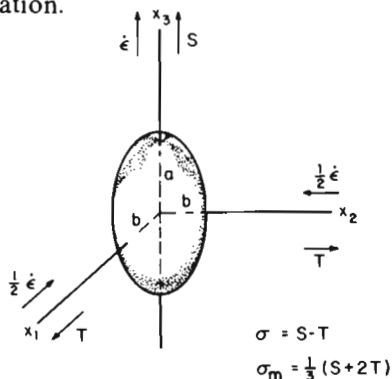Figure 1.1 displays this notation.

FIG. 1.1. Axisymmetric void; remote stresses and strains.

Sections 2 and 3 are devoted to the evolution of a void in the Newtonian viscous solid ($n = 1$) under all possible combinations of S and T. At the beginning of the deformation history the void is taken to be spherical. Depending on the combination of S and T imposed on the block, the void grows or collapses and its shape evolves towards an asymptotic shape which can be characterized as a needle, cylinder, spheroid, or crack. These asymptotic shapes are determined, as are their growth-rates.

Void behavior in the linearly viscous solid is used as a guide in carrying out the analysis of void growth in the nonlinearly viscous solid. Voids with needle-like or cylinder-like shapes are analyzed in Section 4, and the ranges of S and T, for which these shapes are those approached asymptotically by initially spherical voids, are determined. The results of McClintock (1968) for the rigid–perfectly plastic solid are reproduced. Contact is also made with Tracey's (1971) results for cylindrical voids in power-hardening materials.

A detailed analysis of the growth-rate of a spherical void as it depends on n and on S and T is presented in Section 5. The results presented required extensive numerical calculations, but a simple formula derived in Section 6 gives a reasonably accurate approximation for the growth-rate of the void when the remote mean stress exceeds the remote effective stress. In the limit of a rigid–perfectly plastic solid this formula reduces to the Rice and Tracey (1969) formula for high triaxiality conditions.

Some surprising predictions for the deformation of the spherical void are discovered. At high n with $S > T$, the void grows more rapidly perpendicular to the remote straining direction than along it when σ_m is sufficiently large compared to σ. A similar tendency was found by Andersson (1977) for an initially spherical void in a finite cylindrical block with boundary conditions chosen to model high triaxiality conditions at a crack tip. The paper concludes in Section 7 with a brief study of ductile fracture by void growth based on the solutions of Sections 2–6. Estimates of the influence of material nonlinearity and remote stress state on the fracture strain are obtained.

2. Governing Equations for a Void in a Linearly Viscous Solid

An isolated ellipsoidal cavity in an infinite, linearly viscous solid will always remain an ellipsoid under the action of a uniform stress state (constant or variable) at infinity, although it may change its size and shape, and rotate. This fact follows from Eshelby's (1957) paper, and holds for all homogeneous linear relations

$$\sigma_{ij} = L_{ijkl}\dot{\varepsilon}_{kl} \tag{2.1}$$

between strain-rate and stress, including anisotropic ones. (The Eshelby result was for linear elasticity and small strains, but the extension to linearly viscous solids and arbitrary strains is immediate, as long as $\dot{\varepsilon}_{ij}$ is considered to be the current velocity strain.) These results persist for the two-dimensional problems of elliptical cavities in linearly viscous solids analyzed by Berg (1962) and McClintock et al. (1966) in their early studies of void growth and coalescence.

Here we shall consider spheroids (prolate or oblate) of the form

$$(x_1/b)^2 + (x_2/b)^2 + (x_3/a)^2 = 1 \tag{2.2}$$

and study their evolution under the action of the axial and transverse stresses (1.5) lined up

with the axes of the spheroid. We shall ultimately adopt the incompressible, isotropic relation

$$\dot{\varepsilon}_{ij} = \frac{1}{2\eta} s_{ij} \tag{2.3}$$

that follows from (1.3) for $n = 1$. It will be useful, initially, to use the compressible relationship

$$\sigma_{ij} = 2\eta \left(\dot{\varepsilon}_{ij} + \frac{\nu}{1-2\nu} \dot{\varepsilon}_{kk} \delta_{ij} \right) \tag{2.4}$$

and then let the viscous Poisson's ratio ν approach $\frac{1}{2}$ at an appropriate point in the analysis. Symmetry and isotropy imply that the cavity will not rotate, and so we address the problem of calculating its shape and size change. In particular, we shall calculate the strain-rate $\dot{\varepsilon}^l$ in the cavity in terms of S, T, and η, and then, with

$$\dot{a}/a = \dot{\varepsilon}^l_{33} \quad \text{and} \quad \dot{b}/b = \dot{\varepsilon}^l_{11} = \dot{\varepsilon}^l_{22}, \tag{2.5}$$

we shall be able to study the evolution of the void geometry.

Hill (1965) defines the tensor $\mathbf{Q}$ relating the cavity strain-rate to the remote stresses σ^∞ according to

$$\sigma^\infty_{ij} = Q_{ijmn} \dot{\varepsilon}^l_{mn} \tag{2.6}$$

and shows that

$$Q_{ijmn} = L_{ijmn} - L_{ijkl} S_{klmn} \tag{2.7}$$

where $\mathbf{S}$ is the Eshelby (1957) tensor. (Eshelby relates a "stress-free" transformation strain ε^T in an ellipsoidal region of a homogeneous linear elastic material to the actual "constrained" strain ε^c by $\varepsilon^c = S\varepsilon^T$.) In the present spheroidal cavity problem, with $\mathbf{L}$ defined by (2.4) and σ^∞ by (1.5), we find

$$\frac{\sigma_m}{\eta} = \frac{2(1+\nu)}{3(1-2\nu)} \left[(1 - S_{3333} - 2S_{1133}) \dot{\varepsilon}^l_{33} + 2(1 - S_{3311} - S_{1111} - S_{1122}) \dot{\varepsilon}^l_{11} \right], \tag{2.8}$$

$$\frac{\sigma}{3\eta} = \frac{2}{3} \left[(1 - S_{3333} + S_{1133}) \dot{\varepsilon}^l_{33} - (1 + 2S_{3311} - S_{1111} - S_{1122}) \dot{\varepsilon}^l_{11} \right]. \tag{2.9}$$

From Eshelby (1957),

$$\begin{aligned}
8\pi(1-\nu)S_{3333} &= 3a^2 I_{aa} + (1-2\nu)I_a, \\
8\pi(1-\nu)S_{3311} &= 3b^2 I_{ab} - (1-2\nu)I_a, \\
8\pi(1-\nu)S_{1133} &= 3a^2 I_{ab} - (1-2\nu)I_b, \\
8\pi(1-\nu)S_{1111} &= 3b^2 I_{bb} + (1-2\nu)I_b, \\
8\pi(1-\nu)S_{1122} &= 3b^2 I_{bc} - (1-2\nu)I_b,
\end{aligned} \tag{2.10}$$

where, with $\lambda = a/b$,

$$\begin{aligned}
\frac{I_b}{2\pi} \equiv \beta &= \lambda(1-\lambda^2)^{-3/2}\{\cos^{-1}\lambda - \lambda(1-\lambda^2)^{1/2}\}, \quad \lambda < 1, \\
&= \lambda(\lambda^2-1)^{-3/2}\{\lambda(\lambda^2-1)^{1/2} - \cosh^{-1}\lambda\}, \quad \lambda > 1,
\end{aligned} \tag{2.11}$$

and

$$
\begin{aligned}
I_a &= 4\pi - 2I_b, \\
I_{ab} &= [3(a^2 - b^2)]^{-1}(I_b - I_a), \\
I_{aa} &= 4\pi(3a^2)^{-1} - 2I_{ab}, \\
I_{bb} &= 3I_{bc} = \pi b^{-2} - 3I_{ab}/4.
\end{aligned}
\tag{2.12}
$$

Elimination of the components of S in (2.8) using (2.10) and (2.12) gives

$$
S + 2T = \frac{\eta}{\pi} \frac{(1+\nu)}{(1-\nu)} \left[I_b \dot{\varepsilon}_{33}^l + (4\pi - I_b)\dot{\varepsilon}_{11}^l \right].
\tag{2.13}
$$

For the incompressible material ($\nu = 1/2$) this becomes

$$
S + 2T = 3\eta \left[2\beta \dot{\varepsilon}_{33}^l + (4 - 2\beta)\dot{\varepsilon}_{11}^l \right],
\tag{2.14}
$$

where β is defined in (2.11). Similarly, (2.9) reduces to

$$
S - T = 3\eta \left[\alpha \dot{\varepsilon}_{33}^l - \alpha \lambda^{-2} \dot{\varepsilon}_{11}^l \right]
\tag{2.15}
$$

in the incompressible limit where for all $\lambda = a/b$

$$
\alpha = \lambda^2 (\lambda^2 - 1)^{-1}(3\beta - 2).
\tag{2.16}
$$

Inverting (2.14) and (2.15) and noting (2.5), one finds

$$
\eta \frac{\dot{a}}{a} = \frac{\lambda^2 \left[(6 - 5\beta + \alpha)S + 2(\alpha - 2\beta)T \right]}{6\alpha[2\lambda^2 + \beta(1 - \lambda^2)]}
\tag{2.17}
$$

and

$$
\eta \frac{\dot{b}}{b} = \frac{\lambda^2 \left[(\alpha - 2\beta)S + 2(\alpha + \beta)T \right]}{6\alpha[2\lambda^2 + \beta(1 - \lambda^2)]}.
\tag{2.18}
$$

For a given history of S and T, (2.17) and (2.18) govern the evolution of the size and shape of the void. The evolution of the void can also be expressed in terms of the rate of change of its aspect ratio $\lambda = a/b$ and the rate of change of its volume $V = 4\pi ab^2/3$. Since

$$
\frac{\dot{\lambda}}{\lambda} = \frac{\dot{a}}{a} - \frac{\dot{b}}{b}
\tag{2.19}
$$

it follows from (2.17) and (2.18) that

$$
\eta \dot{\lambda} = \frac{\lambda^3 \left[(2 - \beta)S - 2\beta T \right]}{2\alpha[2\lambda^2 + \beta(1 - \lambda^2)]}.
\tag{2.20}
$$

With starting aspect ratio $\lambda_0 = a_0/b_0$ at time $t = 0$, (2.20) provides the time as a function of λ as

$$
\frac{t}{\eta} = \int_{\lambda_0}^{\lambda} \frac{2\alpha[2\lambda^2 + (1 - \lambda^2)\beta]}{\lambda^3[(2 - \beta)S - 2\beta T]} \, d\lambda
\tag{2.21}
$$

assuming S and T do not vary with time. From

$$\frac{\dot{V}}{V} = \frac{\dot{a}}{a} + 2\frac{\dot{b}}{b} \tag{2.22}$$

it also follows that

$$\eta\frac{\dot{V}}{V} = \frac{\lambda^2[(2+\alpha-3\beta)S + 2\alpha T]}{2\alpha[2\lambda^2 + \beta(1-\lambda^2)]}. \tag{2.23}$$

Elimination of time in (2.23) in favor of λ as the dependent variable using (2.20) gives

$$\ln\left[\frac{V}{V_0}\right] = \int_{\lambda_0}^{\lambda} \frac{(2+\alpha-3\beta)S + 2\alpha T}{\lambda[(2-\beta)S - 2\beta T]}\, d\lambda, \tag{2.24}$$

where $V_0 = 4\pi a_0 b_0^2/3$ is the starting volume.

If the void is momentarily a sphere of radius $a = b$, then (2.11) reduces to $\beta = 2/3$, and (2.16) has the limit $\alpha = 2/5$; (2.20) and (2.23) give

$$\eta\dot{\lambda} = \frac{5}{6}(S-T) = \frac{5}{6}\sigma \tag{2.25}$$

and

$$\eta\frac{\dot{V}}{V} = \frac{1}{4}(S+2T) = \frac{3}{4}\sigma_m. \tag{2.26}$$

These results can be restated as

$$\dot{\lambda} = \frac{5}{2}\dot{\varepsilon} \tag{2.27}$$

and

$$\frac{1}{\dot{\varepsilon}}\frac{\dot{V}}{V} = \frac{3}{4}\left[\frac{S+2T}{S-T}\right] \tag{2.28}$$

in terms of the remote strain-rate $\dot{\varepsilon} = \sigma/(3\eta)$ as given by (1.9).

3. Evolution of an Initially Spherical Void under Various S/T in a Linearly Viscous Material

Equation (2.24) relates the evolving aspect ratio and the volume of the void, independently of time and viscosity. This relation holds for time-varying S and T as long as S/T is fixed. In turn, the aspect ratio is related to time and viscosity through (2.20) or (2.21). A differential relation between the aspect ratio and the remote logarithmic strain ε may be obtained immediately from (2.20) and $\dot{\varepsilon} = (S-T)/(3\eta)$ as

$$\frac{d\lambda}{d\varepsilon} = \frac{3\lambda^3[(2-\beta)S - 2\beta T]}{2\alpha(S-T)[2\lambda^2 + \beta(1-\lambda^2)]}, \tag{3.1}$$

and this relation also holds for time-varying S and T if S/T is fixed. Volume histories as functions of remote strain ε may now be calculated parametrically in terms of λ, with V/V_0 obtained from (2.24) and ε found from integration of (3.1).

Figures 3.1(a) through 3.1(g) illustrate what happens to initially spherical voids for all representative combinations of S and T. The chart in Fig. 3.1(a) summarizes the asymptotic shapes and values of V/V_0, λ, a, and b towards which the void evolves. In Figs. 3.1(b) through 3.1(g) the void volume normalized by its starting volume is plotted as a function of the remote stretch in the 3-direction (or its inverse), which is related to the remote logarithmic strain by

$$(L/L_0)_\infty = e^t. \tag{3.2}$$

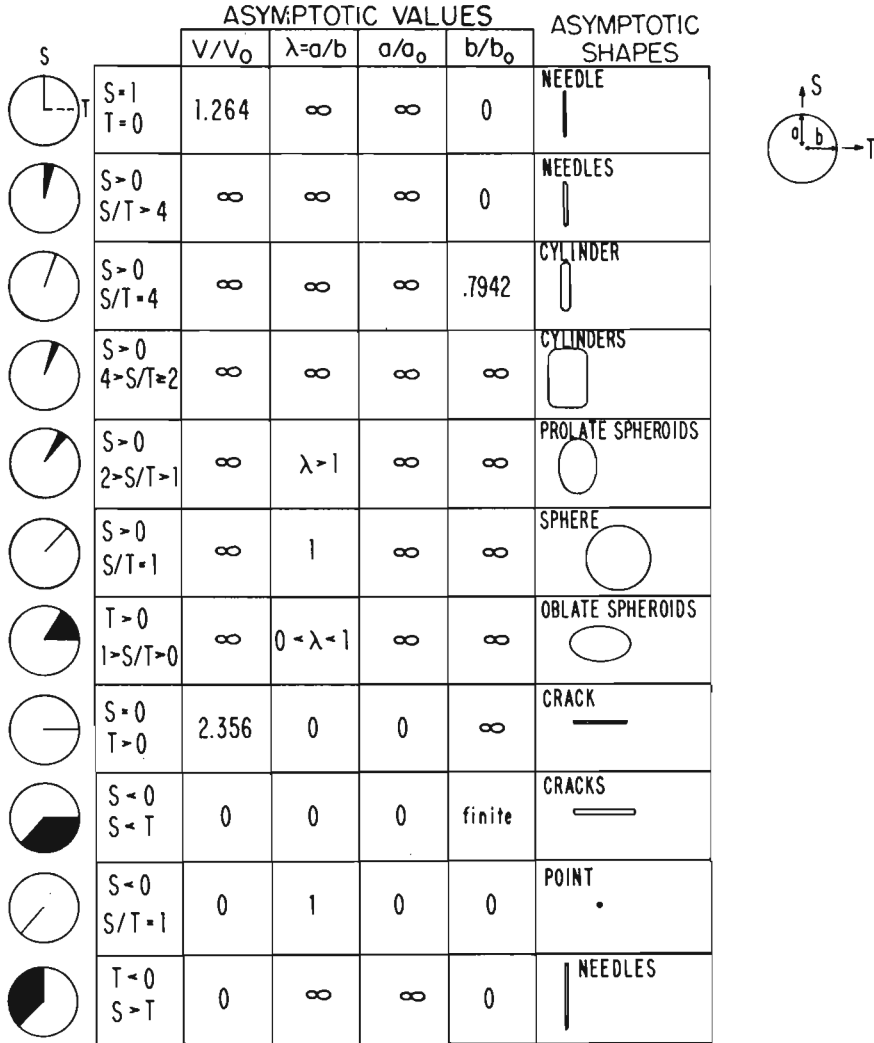| S		ASYMPTOTIC VALUES				ASYMPTOTIC SHAPES
		V/V_0	$\lambda=a/b$	a/a_0	b/b_0	
	$S=1$ $T=0$	1.264	∞	∞	0	NEEDLE
	$S>0$ $S/T>4$	∞	∞	∞	0	NEEDLES
	$S>0$ $S/T=4$	∞	∞	∞	.7942	CYLINDER
	$S>0$ $4>S/T\approx2$	∞	∞	∞	∞	CYLINDERS
	$S>0$ $2>S/T>1$	∞	$\lambda>1$	∞	∞	PROLATE SPHEROIDS
	$S>0$ $S/T=1$	∞	1	∞	∞	SPHERE
	$T>0$ $1>S/T>0$	∞	$0<\lambda<1$	∞	∞	OBLATE SPHEROIDS
	$S=0$ $T>0$	2.356	0	0	∞	CRACK
	$S<0$ $S<T$	0	0	0	finite	CRACKS
	$S<0$ $S/T=1$	0	1	0	0	POINT
	$T<0$ $S>T$	0	∞	∞	0	NEEDLES

FIG. 3.1(a). Asymptotic geometries of initially spherical voids.

Since the material is incompressible, $(L/L_0)_\infty$ is also the inverse of the remote area reduction. The curves in Figs. 3.1(b)–(g) are independent of the time variation of S and T as long as S/T does not change in a given history.

The plots of Figs. 3.1(b)–(g) will be discussed in turn, starting at 12 o'clock in the T-S plane and proceeding clockwise. In Fig. 3.1(b) for $0 \leqslant T/S \leqslant 1/4$ with $S > 0$, the void asymptotes
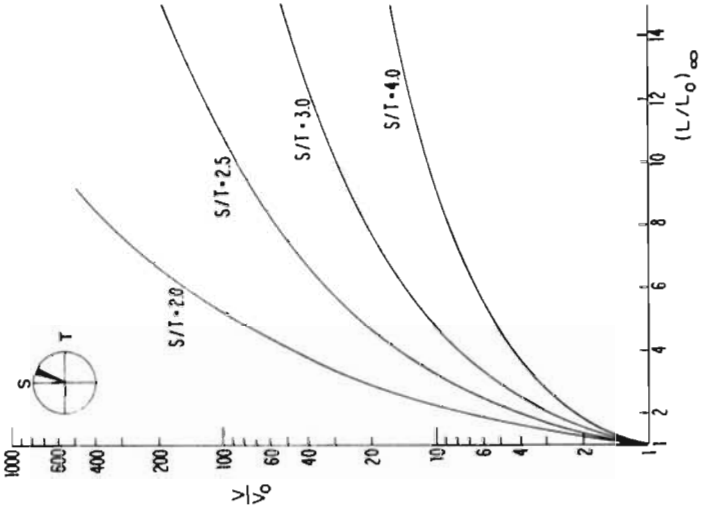
FIG. 3.1(c). Void growth: sphere to cylinder.

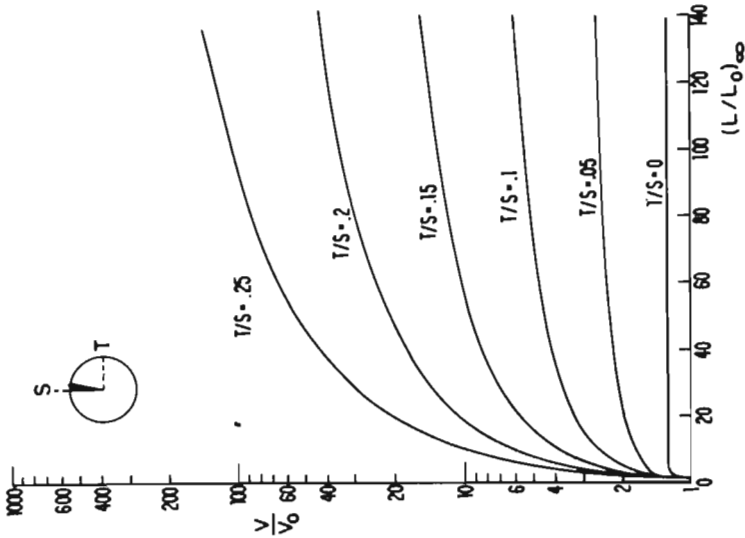
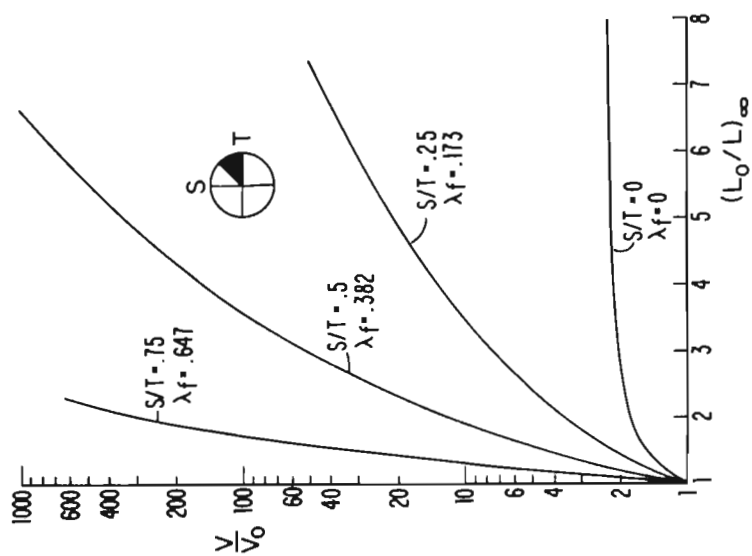FIG. 3.1(b). Void growth: sphere to needle $(T \geq 0, S > 4T)$.

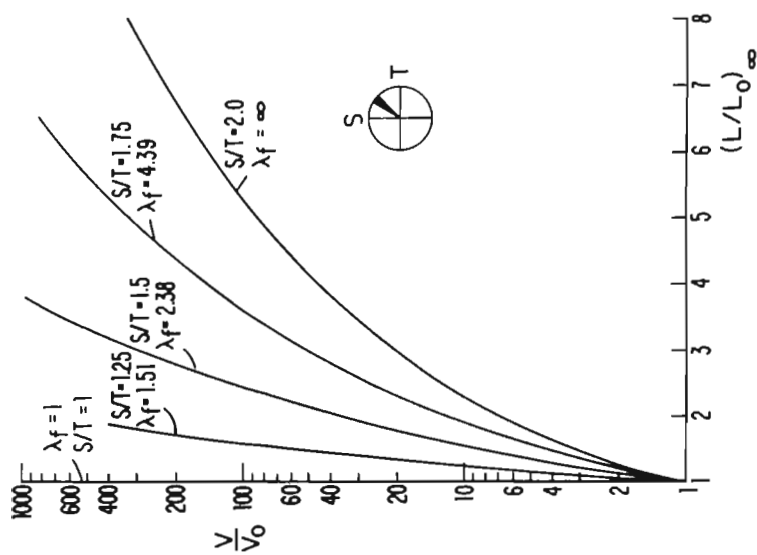FIG. 3.1(e). Void growth: sphere to oblate spheroid.

FIG. 3.1(d). Void growth: sphere to prolate spheroid.
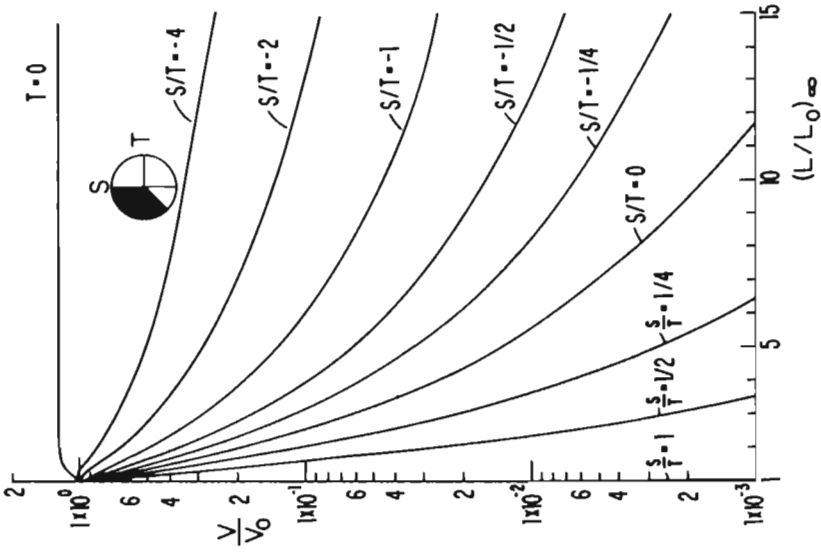
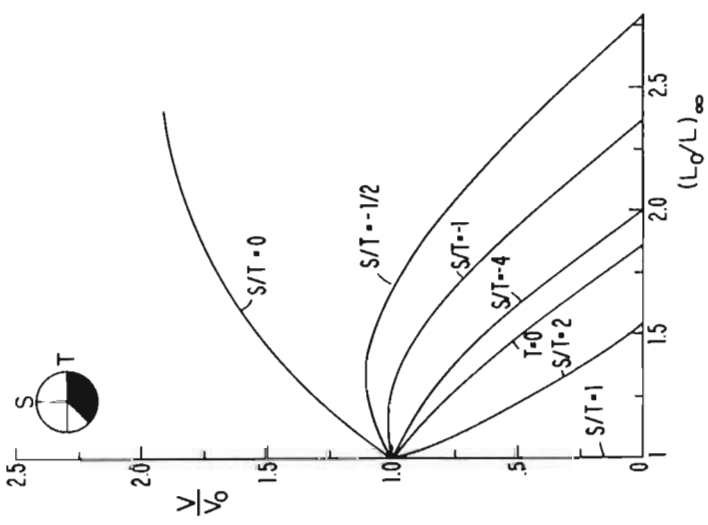FIG. 3.1(g). Void collapse: sphere to needle ($T < 0$, $S > T$).

FIG. 3.1(f). Void collapse: sphere to crack ($S < 0$, $T > S$).

to a needle-like shape of infinite length and zero radius but with infinite volume. Exceptionally for remote uniaxial tension ($S > 0, T = 0$), the volume asymptotes to a value which is only 26.4 % above the starting volume. For $1/4 \leqslant T/S \leqslant 1/2$ with $S > 0$, the void evolves towards a cylinder-like shape of infinite length and radius, except for $T/S = 1/4$, where $b/b_0 \to 0.794$.

For any segment of an infinite cylinder with the x_3-axis as its axis of revolution and subject to remote stresses S and T,

$$\eta \frac{\dot{V}}{V} = \eta \left(\dot{\varepsilon}^I_{33} + 2\dot{\varepsilon}^I_{11} \right) = T \tag{3.3}$$

independent of S. This result, easily found by elementary considerations, agrees with the limit of (2.23) for $a \to \infty$. Equation (3.3) provides the asymptotic value of $\dot{V}/V$ for the range of S and T in which the void asymptotes to a needle or a cylinder, i.e.

$$\eta \frac{\dot{V}}{V} \to \eta \left[\frac{\dot{V}}{V} \right]_f = T \quad (S > 0, 0 \leqslant T/S < 1/2), \tag{3.4}$$

where here and in the sequel a subscript f denotes values associated with an asymptotic shape. As will be seen later, this asymptote also applies in the range $T < 0$ with $S > T$. The bottom two curves in Fig. 3.2 for $S/T = 3$ and $S/T = 4$ show $\dot{V}/V$ as a function of V/V_0 dropping from the starting value (2.26) when the void is spherical to essentially the asymptotic value (3.4) in only a doubling of V over V_0. Thus although the void is still far from a cylinder in appearance, its volume-rate of change is well approximated by its asymptote.
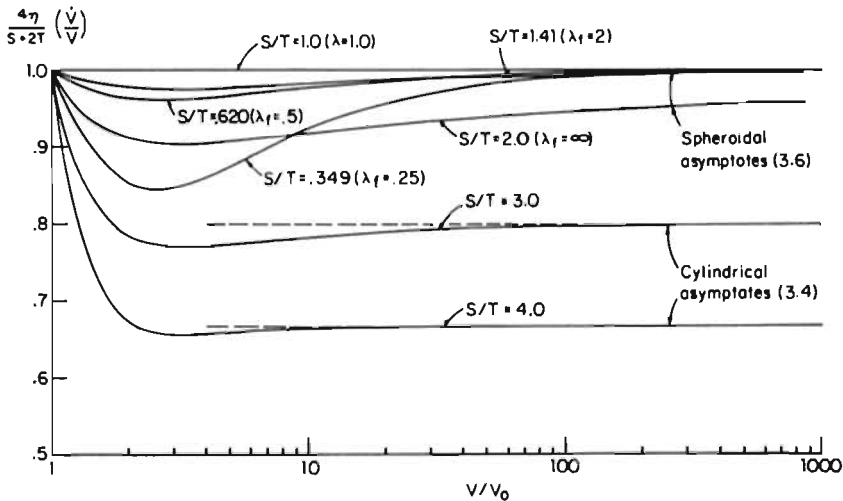

FIG. 3.2. Evolution of void growth rates.

In the range $1 < S/T < 2$ with $T > 0$ the void asymptotes to a prolate spheroid ($\lambda \to \lambda_f > 1$); when $S/T = 1$ the void remains spherical; and for $0 < S/T < 1$ with $T > 0$ the void asymptotes to an oblate spheroid ($\lambda \to \lambda_f < 1$). To discover the asymptotic aspect

ratio λ_f and the associated rate of volume change in the range $0 < S/T < 2$, set $\lambda = 0$ in (2.20) and note

$$\beta \to \beta_f = 2S/(S + 2T).\tag{3.5}$$

The relation between λ_f and S/T plotted in Fig. 3.3 is obtained from (3.5) and (2.11). The asymptotic shape satisfies $\dot{\varepsilon}'_{11} = \dot{\varepsilon}'_{33}$ and, thus, combining (2.14) and (2.22), gives

$$\eta\left[\frac{\dot{V}}{V}\right]_f = \frac{3}{4}\sigma_m = \frac{1}{4}(S + 2T) \quad (0 < S/T < 2).\tag{3.6}$$
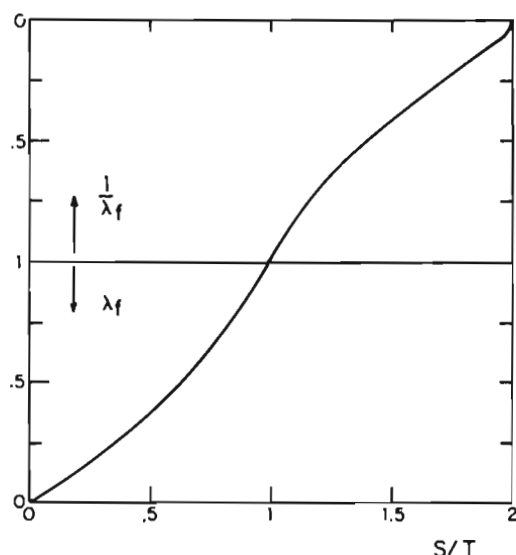

FIG. 3.3. Aspect ratios $\lambda_f = (a/b)_f$ of asymptotic spheroids.

Remarkably, $\eta(\dot{V}/V)_f$ depends only on the remote mean stress, is independent of λ_f, and, moreover, is precisely the same as the starting value (2.26) for the initial spherical shape. At the transition between spheroids and cylinders, where $S/T = 2$, the asymptotic growth-rate (3.6) is continuous with the growth-rate for the cylinder in (3.4). Figure 3.2 shows the extent to which $\dot{V}/V$ departs from (2.26) and (3.6) while the void evolves from the starting spherical shape to the asymptotic shape. For $1 < S/T < 2$, the minimum of $\dot{V}/V$ occurs when the volume has increased to about three times its initial value and never drops below 90% of (3.6). The minimum of $\dot{V}/V$ can be arbitrarily small for sufficiently small S/T, but for $S/T > 0.3$ it does not fall below 80% of (3.6).

When $S < 0$ with $S < T$ in Fig. 3.1(f), the void is crushed to a penny-shaped crack ($a_f = 0$) in the $x_1 - x_2$ plane. With the exception of the case $S = 0$ for which $b/b_0 \to \infty$ and $V/V_0 \to 2.356$, the volume goes to zero and b approaches a finite value at a finite remote strain, as can be determined from the intercept with the abscissa. In uniaxial compression ($S < 0$, $T = 0$) a remote length reduction of about 50% is needed to completely flatten out a spherical void; the final radius of the crack is 1.41 times the radius of the starting sphere.

Finally, for $T < 0$ with $S > T$ in Fig. 3.1(g), the void is crushed to an infinitely long needle ($a \to \infty, b \to 0$) with zero volume. Complete collapse is not attained at finite remote strain but is only approached asymptotically with (3.4) as the asymptote for $\dot{V}/V$. Under transverse pressure alone ($S = 0, T < 0$), an overall area reduction ratio of 12 : 1 is needed to squeeze the void into a needle-like cavity having 0.1 % of its original spherical volume.

Under all-around hydrostatic pressure ($S = T < 0$) the void remains spherical and shrinks to a point. In this case, however, the spherical shape is unstable in that any axisymmetric departure from sphericity will drive the void to either a penny-shaped crack with finite radius or a needle with finite length, both with zero volume. Similarly, the asymptotic shapes found in the tensile range, $0 < S/T < 2$, are also possible solutions when the signs of both S and T are reversed. In fact, if the void started with the asymptotic aspect ratio λ_f rather than as a sphere, the aspect ratio would remain unchanged as the void collapsed to a point. However, it is easy to show that these shapes are unstable in compression, just as in the case of the spherical void when $S = T < 0$.
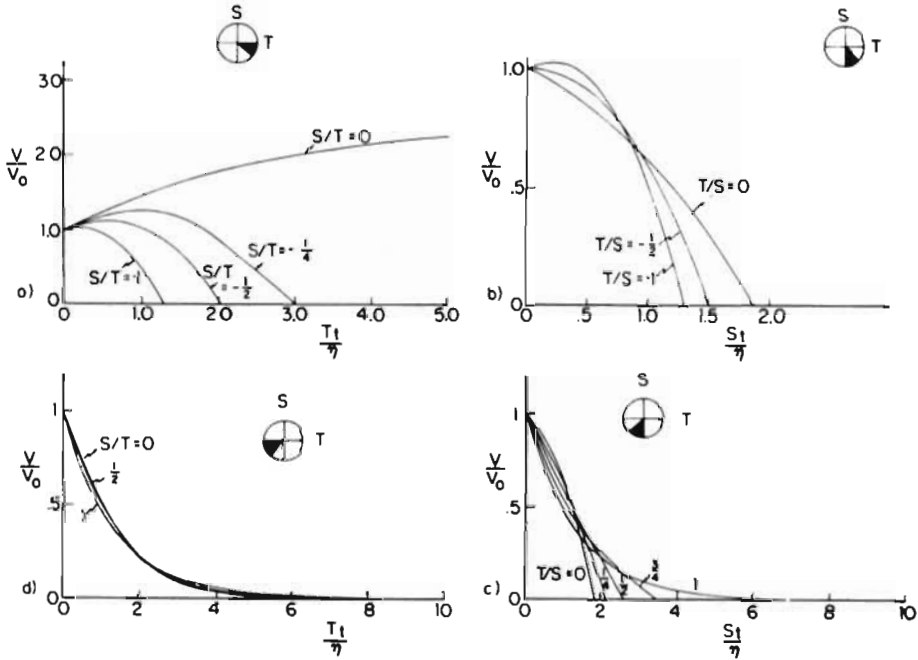

FIG. 3.4. Void-volume time histories, $S \leqslant 0$.

Time histories of the volume for $S < 0$ are shown in Fig. 3.4. Here use is made of (2.21) and it is now assumed that S and T are time-independent. For $S < 0$ and $T > S$ (Figs. 3.4(a) through 3.4(c)) $V \to 0$ at finite time; for $S < 0$ and $T \leqslant S$, $V \to 0$ as $t \to \infty$. The nearly identical responses in Fig. 3.4(d) for $0 \leqslant S/T \leqslant 1$ reflect the fact that the void very quickly assumes the asymptotic growth-rate (3.4) for the cylinder or needle.

4. Deformation of an Infinite Cylindrical Void in a Nonlinearly Viscous Material

Let the axis of an infinite cylindrical void of radius b coincide with the x_3-axis. The surface of the void is traction-free, while far from the void the stresses are specified by S and T as in (1.5). Surrounding the void is the incompressible, nonlinearly viscous material (1.3). Solutions to this problem have been given by McClintock (1968) and Rice and Tracey (1969) for the rigid–plastic limit ($n = \infty$) and by Tracey (1971) for arbitrary values of n. The solution presented here is in a form which is particularly simple and appropriate for the void growth problem. In addition, the solution will be used to infer the ranges of S/T corresponding to needles or cylinders as asymptotic shapes.

In a cylindrical coordinate system (r, θ, z) the nonzero in-plane velocity component is $v_r(r)$ and the nonzero strain-rate components are

$$\dot{\varepsilon}_r = \frac{dv_r}{dr}, \quad \dot{\varepsilon}_\theta = \frac{1}{r}v_r, \quad \dot{\varepsilon}_z = \dot{\varepsilon}, \tag{4.1}$$

where $\dot{\varepsilon}$ is given by (1.9). Incompressibility requires

$$\frac{dv_r}{dr} + \frac{1}{r}v_r = -\dot{\varepsilon} \tag{4.2}$$

from which it follows that

$$v_r = Ar^{-1} - \tfrac{1}{2}r\dot{\varepsilon} \tag{4.3}$$

and

$$\dot{\varepsilon}_r = -Ar^{-2} - \tfrac{1}{2}\dot{\varepsilon}, \tag{4.4}$$

$$\dot{\varepsilon}_\theta = Ar^{-2} - \tfrac{1}{2}\dot{\varepsilon}, \tag{4.5}$$

where A is a free amplitude factor.

Equilibrium requires

$$\frac{d\sigma_r}{dr} + \frac{\sigma_r - \sigma_\theta}{r} = 0. \tag{4.6}$$

But from (1.3) and (4.4),

$$\sigma_r - \sigma_\theta = 2\eta\sigma_e^{1-n}(\dot{\varepsilon}_r - \dot{\varepsilon}_\theta) = -4\eta Ar^{-2}(3\eta\dot{\varepsilon}_e)^{(1-n)/n} \tag{4.7}$$

where

$$\dot{\varepsilon}_e \equiv (2\dot{\varepsilon}_{ij}\dot{\varepsilon}_{ij}/3)^{1/2} = (4A^2r^{-4}/3 + \dot{\varepsilon}^2)^{1/2}. \tag{4.8}$$

Substitution of (4.7) into (4.6) and integration of (4.6) from $r = b$, where $\sigma_r = 0$, to $r = \infty$, where $\sigma_r = T$, gives

$$T = (3\eta)^{1/n}(4A/3)\int_b^\infty (4A^2r^{-4}/3 + \dot{\varepsilon}^2)^{(1-n)/2n}r^{-3}dr. \tag{4.9}$$

By (1.9), this can be rewritten as

$$\frac{T}{S-T} = \frac{4A}{3\dot{\varepsilon}}\int_b^\infty \left[1 + \left(\frac{2A}{\sqrt{3}\dot{\varepsilon}}\right)^2 r^{-4}\right]^{(1-n)/2n} r^{-3}dr. \tag{4.10}$$

Lastly, with the change of integration variable

$$x = \omega\left(\frac{b}{r}\right)^2, \quad \text{where} \quad \omega = \frac{2A}{\sqrt{3}\dot{\varepsilon}b^2}, \tag{4.11}$$

(4.10) gives the final result

$$\frac{S}{T} = 1 + \left[\frac{1}{\sqrt{3}}\int_0^\omega (1+x^2)^{(1-n)/2n}dx\right]^{-1}. \tag{4.12}$$

The rate of volume change of a segment of the cylindrical void with current length L is

$$\dot{V} = 2\pi Lb\dot{b} + \pi b^2\dot{L} = 2\pi LA, \tag{4.13}$$

where the last equality follows from (4.4) and $\dot{\varepsilon}_\theta = \dot{b}/b$, $\dot{\varepsilon} = \dot{L}/L$ at the cavity. Therefore

$$\frac{1}{\dot{\varepsilon}}\frac{\dot{V}}{V} = \frac{2A}{\dot{\varepsilon}b^2} = \sqrt{3}\omega \tag{4.14}$$

and consequently (4.12) with (4.14) provides the desired relation between S/T and $\dot{V}/(\dot{\varepsilon}V)$.

For the linearly viscous material ($n = 1$), (4.12) integrates to

$$\frac{1}{\dot{\varepsilon}}\frac{\dot{V}}{V} = \frac{3T}{S-T} \tag{4.15}$$

in agreement with the result obtained by combining (3.4) and (1.9). For a rigid-perfectly plastic material ($n = \infty$), (4.12) can be integrated to give McClintock's (1968) formula

$$\frac{1}{\dot{\varepsilon}}\frac{V}{V} = \sqrt{3}\sinh\left(\frac{\sqrt{3}T}{S-T}\right). \tag{4.16}$$

This formula brings out the large amplification of the volume growth-rate when triaxiality is high, i.e. when $T \gg S-T$ or, equivalently, when $\sigma_m \gg \sigma$. The formula is valid for arbitrary signs of S and T, and high hydrostatic pressure in combination with remote straining $\dot{\varepsilon}$ has a correspondingly large effect on the rate of void collapse.

The solution (4.12) can be used to infer whether a void which starts as a sphere, say, will evolve to an asymptotic shape which is a cylinder or needle. First, suppose S and T are in the range in which the void asymptotes to a cylindrical void, which as previously defined requires that $a/b \rightarrow \infty$ with $b \geqslant 0$. If the void is to asymptote to a cylindrical void, the cylinder solution must for consistency grow in radius, or at least not decrease in radius, but in such a way that its elongation per unit length is even more rapid. That is, for S and T in the range such that the cylindrical void solution satisfies

$$0 \leqslant \frac{1}{\dot{\varepsilon}}\frac{\dot{b}}{b} < 1 \quad \text{with} \quad \dot{\varepsilon} > 0, \tag{4.17}$$

the asymptotic shape is expected to be a cylinder. By a similar argument the asymptotic shape will be a needle ($b \rightarrow 0$, $a \rightarrow \infty$) when

$$\frac{1}{\dot{\varepsilon}}\frac{\dot{b}}{b} < 0 \quad \text{with} \quad \dot{\varepsilon} > 0. \tag{4.18}$$

From (4.13) and (4.14),

$$\frac{1}{\dot{\varepsilon}}\frac{\dot{b}}{b} = \frac{1}{2}\left(\frac{1}{\dot{\varepsilon}}\frac{\dot{V}}{V} - 1\right) = \frac{1}{2}(\sqrt{3}\omega - 1). \tag{4.19}$$

The transition of the asymptotic shapes from needles to cylinders occurs when

$$\frac{\dot{b}}{\dot{\varepsilon}b} = 0 \quad \text{or} \quad \frac{\dot{V}}{\dot{\varepsilon}V} = \sqrt{3}\omega = 1, \tag{4.20}$$

which from (4.12) corresponds to

$$S/T = 1 + \sqrt{3}\left[\int_0^{1/\sqrt{3}} (1 + x^2)^{(1-n)/2n}dx\right]^{-1}. \tag{4.21}$$

For $n = 1$ (4.21) gives $S/T = 4$ and, for $n = \infty$, $S/T = 4.153$. A plot of the transition values of S/T as a function of n is shown in Fig. 4.1. The transition between asymptotic shapes which are cylinders and those which are pseudo-spheroids occurs when

$$\frac{\dot{b}}{\dot{\varepsilon}b} = 1 \quad (\dot{\varepsilon} > 0) \quad \text{or} \quad \frac{\dot{V}}{\dot{\varepsilon}V} = \sqrt{3}\omega = 3, \tag{4.22}$$

whence

$$S/T = 1 + \sqrt{3}\left[\int_0^{\sqrt{3}} (1 + x^2)^{(1-n)/2n}dx\right]^{-1}. \tag{4.23}$$

For $n = 1$, (4.23) gives $S/T = 2$, and, for $n = \infty$, $S/T = 2.315$; the results for intermediate values of n are shown in Fig. 4.1.
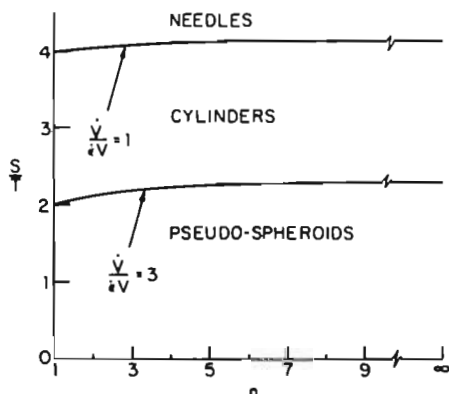

FIG. 4.1. Transition boundaries ($S > 0$), pseudo-spheroids to cylinders to needles.

5. Deformation-rate of a Spherical Void in a Nonlinearly Viscous Solid

The initial rates of deformation and dilatation of a spherical void in an infinite block of the incompressible, nonlinearly viscous solid characterized by (1.3) is studied in this Section. As

in the linear problem, the block is subject to the remote stresses (1.5), but now attention will be directed mainly to the effects of axial and transverse stresses S and T that are either both positive or both negative.

The minimum principle for velocities stated by Hill (1956) will be generalized to a form appropriate for infinite domains, and then used to find approximate Rayleigh–Ritz solutions. Consider a traction-free void of arbitrary shape inside a finite spherical region whose radius R will subsequently be permitted to become unbounded. The outer spherical surface is denoted by S_R, its outward unit normal by $\mathbf{n}$, and tractions $T_i = \sigma_{ij}^\infty n_j$ consistent with the uniform stress state σ^∞ given by (1.5) are imposed on S_R. The material region surrounding the void and contained within S_R is denoted by V_R. Then (Hill, 1956) the velocities v_i minimize the functional

$$\Phi = \int_{V_R} W(\dot{\varepsilon})\,dV - \int_{S_R} \sigma_{ij}^\infty n_i v_j\,dS, \tag{5.1}$$

where the usual admissibility conditions

$$v_{i,i} = 0, \quad \dot{\varepsilon}_{ij} = \tfrac{1}{2}(v_{i,j} + v_{j,i}), \tag{5.2}$$

are imposed, and

$$W(\dot{\varepsilon}) = \int_0^t \sigma_{ij}\,d\dot{\varepsilon}_{ij} = (3\eta)^{1/n}\left(\frac{n}{n+1}\right)(\dot{\varepsilon}_e)^{(n+1)/n}, \tag{5.3}$$

where

$$\dot{\varepsilon}_e = (2\dot{\varepsilon}_{ij}\dot{\varepsilon}_{ij}/3)^{1/2}. \tag{5.4}$$

Here $\dot{\varepsilon}_e$ is an effective strain-rate which, from (1.3), is related to σ_e according to the simple tension formula (1.1).

Now let

$$v_i = v_i^\pi + \bar{v}_i \quad \text{and} \quad \dot{\varepsilon}_{ij} = \dot{\varepsilon}_{ij}^\infty + \dot{\bar{\varepsilon}}_{ij}, \tag{5.5}$$

where $\mathbf{v}^\infty$ and $\dot{\varepsilon}^\infty$ are the velocity and uniform strain-rates due to σ^∞ in the absence of the void and where

$$\dot{\bar{\varepsilon}}_{ij} = \tfrac{1}{2}(\bar{v}_{i,j} + \bar{v}_{j,i}), \quad \bar{v}_{k,k} = 0. \tag{5.6}$$

The minimum principle remains valid if the Φ in (5.1) is replaced by

$$\Phi = \int_{V_R} [W(\dot{\varepsilon}) - W(\dot{\varepsilon}^\pi)]\,dV - \int_{S_R} \sigma_{ij}^\infty n_j \bar{v}_i\,dS \tag{5.7}$$

and this new Φ is minimized with respect to the additional velocity field $\bar{\mathbf{v}}$. Next, by the principle of virtual work,

$$\int_{S_R} \sigma_{ij}^\infty n_j \bar{v}_i\,dS = \int_{V_R} \sigma_{ij}^\infty \dot{\bar{\varepsilon}}_{ij}\,dV + \int_S \sigma_{ij}^\infty n_j \bar{v}_i\,dS, \tag{5.8}$$

where $\mathbf{n}$ is the unit normal to the void surface S pointing into V_R. Thus, (5.7) can be written as

$$\Phi = \int_{V_R} [W(\dot{\varepsilon}) - W(\dot{\varepsilon}^\infty) - \sigma_{ij}^\infty \dot{\bar{\varepsilon}}_{ij}]\,dV - \int_S \sigma_{ij}^\infty n_j \bar{v}_i\,dS. \tag{5.9}$$

It is now possible to let the outer radius R become infinite. For $x \to \infty, \dot{\varepsilon} \to 0$, and

$$W(\dot{\varepsilon}) - W(\dot{\varepsilon}^{\infty}) - \sigma_{ij}^{\infty} \dot{\varepsilon}_{ij} = O(\dot{\varepsilon}_{ij} \dot{\varepsilon}_{ij}). \tag{5.10}$$

Thus the volume integral in (5.9) is well defined for $R \to \infty$ for all additional strains which satisfy

$$\dot{\varepsilon} = o(r^{-s}) \quad \text{as} \quad r \equiv (x_i x_i)^{1/2} \to \infty, \quad \text{where} \quad s > 3/2. \tag{5.11}$$

In the linear problem ($n = 1$) for the spherical void, $\dot{\varepsilon} \sim r^{-3}$ for large r. For the spherically symmetric solution with $S = T$, $\dot{\varepsilon} \sim r^{-3}$ for large r for all n and (5.9) is well defined even though $\dot{\varepsilon}^{\alpha} = 0$.

In the rigid–perfectly plastic limit, (5.9) continues to apply, but σ^{α} must satisfy $s_{ij}' s_{ij}' = 2\sigma_0^2/3$. In this limit, the minimum principle reduces to the one used by Rice and Tracey (1969) in their rigid–plastic analysis. For finite n a principle suitable for infinite domains that is essentially the same as the one derived here was communicated to one of us (B.B.) by J. R. Rice in 1967.

5.1. *Spherically symmetric solution* $(S = T)$

We digress briefly to give the solution for the case in which the remote stress conditions are equivalent to hydrostatic pressure or tension ($\sigma_m = S = T$). We shall also give the solution for the spherical void in a finite spherical region with outer radius R since this simple solution brings out the strong influence of the void volume fraction when the material is nonlinear.

The strain-rate components of a spherically symmetric solution in a spherical coordinate system (r, θ, ϕ) are related to the radial velocity $v_r(r)$ by

$$\dot{\varepsilon}_r = v_{r,r}, \quad \dot{\varepsilon}_{\theta} = \dot{\varepsilon}_{\phi} = r^{-1} v_r. \tag{5.12}$$

Incompressibility requires $v_{r,r} + 2r^{-1} v_r = 0$, which implies that the most general spherically symmetric velocity is

$$v_r = Ar^{-2}. \tag{5.13}$$

With the aid of (1.3) and (5.12), the radial equilibrium equation can be integrated subject to $\sigma_r = 0$ at $r = a$ and $\sigma_r = \sigma_m$ at $r = R$. The equation for A which results is

$$A = \text{sign}\,(\sigma_m) \frac{a^3}{6\eta} \left[\frac{3}{2n} |\sigma_m| \right]^n \left[1 - \rho^{1/n} \right]^{-n}, \tag{5.14}$$

where $\rho = (a/R)^3$ is the ratio of void volume to total volume. The dilatation rate of the void is $\dot{V}/V = 3v_r(a)/a$, and so we have

$$\eta \frac{\dot{V}}{V} = \tfrac{1}{2} \text{sign}\,(\sigma_m) \left[\frac{3}{2n} |\sigma_m| \right]^n \left[1 - \rho^{1/n} \right]^{-n}. \tag{5.15}$$

The influence of void volume fraction on the dilatation rate is seen by expanding (5.15) in terms of small ρ:

$$\eta \frac{\dot{V}}{V} = \frac{1}{2} \text{sign}\,(\sigma_m) \left[\frac{3}{2n} |\sigma_m| \right]^n \left[1 + n\rho^{1/n} + \ldots \right]. \tag{5.16}$$

Note that the lowest order influence of the nonzero void volume fraction enters as $\rho^{1/n}$. A void volume fraction of only one-tenth of 1% ($\rho = 10^{-3}$) already increases $\dot{V}$ by almost 30%

above the prediction for the infinite region ($\rho = 0$) when $n = 3$. Interaction effects between voids are therefore expected to be significant at relatively low volume fractions for the nonlinear materials, and this must be borne in mind in any attempts to use solutions for the isolated void in an infinite block to make predictions for porous media. Conversely, numerical calculations carried out for finite blocks of material cannot be expected to reflect accurately the behavior of a void in an infinite block unless the void volume fraction is extremely small.

5.2. Numerical solution ($S \neq T$)

For $\sigma = S - T \neq 0$, a Rayleigh–Ritz method based on the minimum principle was used to generate approximate solutions in the nonlinearly viscous range, including the rigid–perfectly plastic limit. Attention will be focused on the results for the rates of volume change of the voids and for the character of their changes from an initially spherical shape.

A general representation of the incompressible, axisymmetric additional velocity field can be written in terms of a stream function $\chi(r, \theta)$ as

$$\tilde{v}_r = -r^{-2}(\sin\theta)^{-1}(\chi\sin\theta)_{,\theta}, \quad \tilde{v}_\theta = r^{-1}\chi_{,r}. \tag{5.17}$$

For a field which is symmetric with respect to $\theta = \pi/2$ ($x_3 = 0$), χ can be expressed as

$$\chi(r, \theta) = A\cot\theta + \sum_{k=2,4,\ldots} P_{k,\theta}(\cos\theta)f_k(r), \tag{5.18}$$

where $P_k(\cos\theta)$ is the Legendre polynomial of degree k. The first term in (5.18) generates the spherically symmetric contribution (5.13) to the field. The amplitude A and the unknown functions $f_k(r)$ must be chosen to minimize Φ in (5.9). From (5.17)

$$\tilde{v}_r = Ar^{-2} + \sum_{k=2,4,\ldots} n(n+1)P_k(\cos\theta)r^{-2}f_k(r) \tag{5.19}$$

and

$$\tilde{v}_\theta = \sum_{k=2,4,\ldots} P_{k,\theta}(\cos\theta)r^{-1}f_{k,r}(r). \tag{5.20}$$

The rate of change of void volume is given by

$$\dot{V} = \int_S v_r \, dS = 4\pi A \quad \text{or} \quad \dot{V}/V = 3Aa^{-3} \tag{5.21}$$

and is thus uniquely tied to the spherically symmetric field.

The functions $f_k(r)$ were approximated by a finite number of terms according to

$$f_k(r) = \sum_{i=1} A_k^{(i)}r^{2-i} = A_k^{(1)}r + A_k^{(2)} + A_k^{(3)}r^{-1} + A_k^{(4)}r^{-2} + \ldots. \tag{5.22}$$

Expressions for the associated additional strain-rates are readily derived from

$$\dot{\tilde{\varepsilon}}_r = \tilde{v}_{r,r}, \quad \dot{\tilde{\varepsilon}}_\theta = r^{-1}\tilde{v}_{\theta,\theta} + r^{-1}\tilde{v}_r, \quad \dot{\tilde{\varepsilon}}_\phi = -\dot{\tilde{\varepsilon}}_r - \dot{\tilde{\varepsilon}}_\theta,$$
$$\dot{\tilde{\varepsilon}}_{r\theta} = \tfrac{1}{2}(r^{-1}\tilde{v}_{r,\theta} - r^{-1}\tilde{v}_\theta + \tilde{v}_{\theta,r}). \tag{5.23}$$

For convenience, the amplitude factors A and $A_k^{(i)}$ $(k = 2, 4, \ldots; i = 1, 2, \ldots)$ are denoted collectively by $\{A_j\}$, and these are the variables with respect to which Φ must be minimized. For prescribed S and T, Φ in (5.9) is

$$\Phi(\{A_j\}) = 4\pi \int_a^\alpha r^2\, dr \int_0^{\pi/2} \sin\theta [W(\dot{\varepsilon}) - W(\varepsilon^\infty) - \sigma_{ij}^\infty \dot{\varepsilon}_{ij}] d\theta$$
$$- 4\pi a^2 \int_0^{\pi/2} \sigma_{ij}^\infty n_j \dot{v}_i \sin\theta\, d\theta \qquad (5.24)$$

and the last integral in (5.24) is just

$$4\pi a^2 \int_0^{\pi/2} \sigma_{ij}^\alpha n_j \dot{v}_i \sin\theta\, d\theta = 4\pi\sigma_m A + \frac{8\pi}{5}\sigma \sum_i A_2^{(i)} a^{2-i}(4-i). \qquad (5.25)$$

The double integral in (5.24) cannot be evaluated analytically in terms of the amplitude factors except in the spherically symmetric case when A is the only nonzero factor or when $n = 1$. Minimization of Φ with respect to these amplitude factors was achieved by a numerically implemented Newton–Raphson method. By the change of variable $\mu = a/r$, the r-integration in the double integral was converted to an integration over the range $0 \leqslant \mu \leqslant 1$. At each of ten Gaussian integration stations of μ, the inner integration with respect to θ was carried out (for assigned values of the A_j's) with a ten-point Gaussian quadrature formula. These values were then used in the ten-point formula for the outer integration with respect to μ. The accuracy of the scheme was checked against the exact evaluation of Φ for $n = 1$ and for the spherically symmetrical case for general n. In all cases checked, the numerical integration gave Φ to five or six significant figures.

For a given set of N amplitude factors the minimum condition is

$$\partial\Phi/\partial A_j = 0, \quad j = 1, \ldots, N. \qquad (5.26)$$

With $\{A_j\}$ as an estimate of the solution to (5.26), the improved Newton–Raphson estimate $\{A_j + \Delta A_j\}$ is obtained from

$$\sum_{m=1}^N \Delta A_m \partial^2\Phi/\partial A_m \partial A_j = -\partial\Phi/\partial A_j, \qquad (5.27)$$

where the partial derivatives are evaluated at $\{A_j\}$. All partial derivatives were found numerically from finite difference formulas such as

$$\frac{\partial\Phi}{\partial A_j} = \frac{\Phi(A_1, \ldots, A_j + \delta, \ldots) - \Phi(A_1, \ldots, A_j - \delta, \ldots)}{2\delta}. \qquad (5.28)$$

The scheme proved highly effective and displayed the quadratic convergence characteristic of this method in the vicinity of the minimum.

The choice of functions used for the representation of $\chi(r, \theta)$ in (5.18) and (5.22) was guided by the results of trial calculations aimed at reaching the minimum of Φ most efficiently. In addition to the spherically symmetric term, the P_2 terms are the most important, and in some of our exploratory calculations as many as six free amplitude factors $(A_2^{(i)}, i = 1, \ldots, 6)$ were used to represent $f_2(r)$ in (5.22). Of these six, $A_2^{(2)}$, $A_2^{(3)}$ and $A_2^{(4)}$ were found to be more important than any other set of three and led to results which were not appreciably different from those obtained with the full set of six. Our final choice of χ, which was used in

determining most of the numerical results presented below, was

$$\chi(r, \theta) = A \cot \theta + P_{2,\theta}(\cos \theta) \left[A_2^{(2)} + A_2^{(3)} r^{-1} + A_2^{(4)} r^{-2} \right]$$
$$+ P_{4,\theta}(\cos \theta) \left[A_4^{(2)} + A_4^{(3)} r^{-1} + A_4^{(4)} r^{-2} \right], \tag{5.29}$$

with a total of seven free amplitude factors.

The numerical minimization procedure gave results for the linear case ($n = 1$) which were accurate to six significant figures. However, this accuracy reflects mainly on the numerical evaluation of Φ since (5.29) contains the exact solution when $n = 1$, i.e.

$$A = \frac{1}{4\eta} a^3 \sigma_m, \quad A_2^{(2)} = -\frac{5}{3} A_2^{(4)} a^2 = \frac{5}{54\eta} a^3 \sigma, \tag{5.30}$$

with the other amplitudes zero. For $n > 1$, the terms containing P_4 have a minor quantitative influence on the shape change but are not crucial as far as qualitative predictions are concerned. A form of parameter tracking was used to generate numerical results. For a given S and T, the solution for $n = 1$ was used as the first guess of the solution at a somewhat larger n and when that solution had been found it, in turn, was used as the first guess for a yet higher n. Calculations for $n = \infty$ were carried out separately.

As a check on our numerical method and to make contact with the analysis of Rice and Tracey (1969), we specialized our scheme to the rigid–perfectly plastic limit ($n = \infty$) and studied the results of choosing the same approximating functions used by Rice and Tracey. Their analyses only involved two degrees of freedom: the amplitude A of the spherically symmetric field and the amplitude of a P_2 term with a fixed, associated r-variation $f_2(r)$. They did, however, repeat their calculations for six choices of $f_2(r)$. Our specialization to the choices of Rice and Tracey did reproduce their numerical results in all cases checked. While $\dot{V}$ was only slightly affected by the choice of $f_2(r)$, Rice and Tracey found substantial variation in the corresponding shape changes. For convenience, let us denote the rate of change of the vertical axis of the spherical void by $\dot{a}$ and let $\dot{b}$ be the rate of change of the equatorial radius. For $\sigma_m > \sigma > 0$, Rice and Tracey found that for four of their r-variations, the shape became prolate ($\dot{a} > \dot{b}$), while for the other two $f_2(r)$ choices it became oblate ($\dot{a} < \dot{b}$). Rice and Tracey discounted the possibility of evolution towards an oblate shape in the presence of a positive axial strain-rate at infinity and attributed this anomalous prediction to poor choices for $f_2(r)$. They evidently did not note, however, that the two "poor" choices gave lower values for the minimum of Φ than did some of the other four choices. It will be seen that for $n > 1$ evolution towards an oblate shape is the rule rather than the exception when $\sigma > 0$ and the triaxiality ratio σ_m/σ is high.

Numerical results obtained by minimizing Φ with respect to the seven amplitudes in (5.29) will now be presented. Figures 5.1(a) and 5.1(b) give plots of $\dot{V}/(\dot{\varepsilon} V)$ as a function of σ_m/σ for the case when both σ_m and σ are positive (i.e. $S + 2T > 0$ and $S > T$) or are both negative. The solid line curves are the numerical results obtained from (5.29). As already mentioned, $\dot{V}$ is only weakly dependent on a wide variety of choices in approximating functions when $\sigma_m/\sigma > 1$. In fact, for sufficiently large σ_m/σ, accurate results for V are obtained by using just the spherically symmetric term, and the dashed line curves in Fig. 5.1(b) are based on an approximate formula derived under this assumption in Section 6. The dashed line curve for the rigid–perfectly plastic solid ($n = \infty$) coincides with the corresponding high triaxiality approximation of Rice and Tracey (1969).
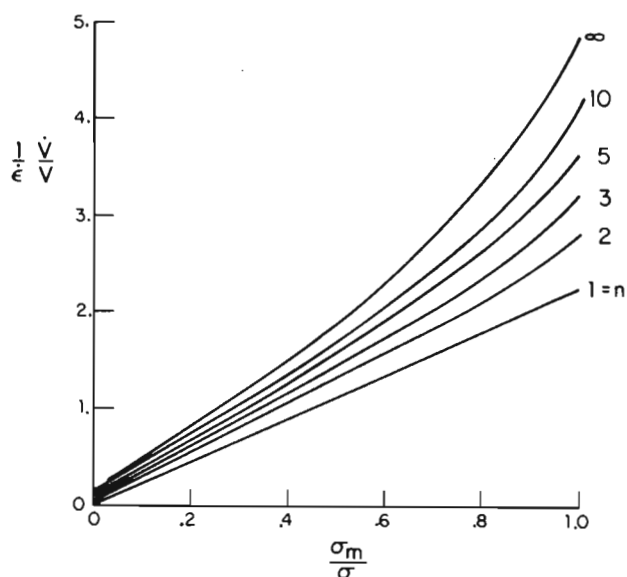
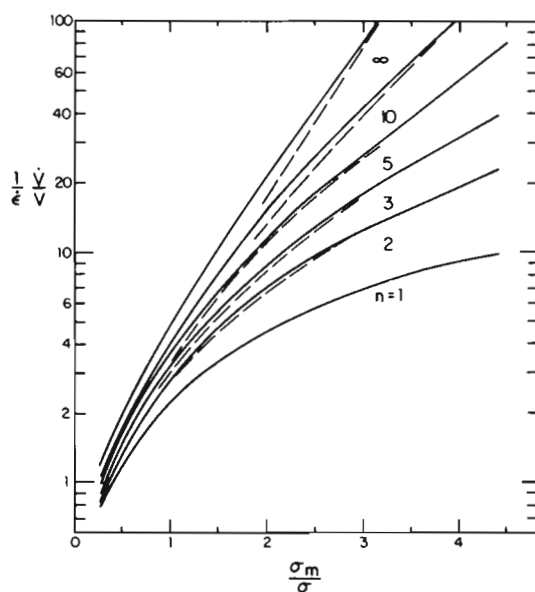FIG. 5.1(a). Dilatation rate of spherical void, low triaxiality.

FIG. 5.1(b). Dilatation rate of spherical void, moderate to high triaxiality.

We note from Fig. 5.1(b) that nonlinearity plays an exceptionally strong role in the expansion (or contraction) of the volume growth-rate of the void, as measured by $\dot{V}/(\dot{\epsilon}V)$, in the high triaxiality range where $\sigma_m/\sigma > 1$. A similar conclusion was drawn by Hellan (1975)

on the basis of a high triaxiality approximation not unlike that which will be discussed in Section 6.

Numerical results related to the shape change of the spherical void are shown in Fig. 5.2, where curves of $\dot{a}/\dot{b}$ are plotted against S/T for the case in which S and T are both positive (or both negative). For the linearly viscous solid $(n = 1)$,

$$\frac{\dot{a}}{\dot{b}} = \frac{9\sigma_m + 20\sigma}{9\sigma_m - 10\sigma} = 1 + \frac{30(S - T)}{16T - 7S}, \tag{5.31}$$

and the void grows towards a prolate shape when $0 < T < S$ and towards an oblate shape when $0 < S < T$, as has already been discussed in Section 3. In contrast, a spherical void in a rigid–perfectly plastic solid $(n = \infty)$ grows towards an oblate shape when $0 < T < S < 1.85T$, and $\dot{b}$ can be more than twice $\dot{a}$. This seemingly anomalous effect is biggest at high n and essentially disappears for n less than 2. For $0 < S < T$ the situation reverses with the void becoming prolate in the nonlinear material for S/T sufficiently close to unity.
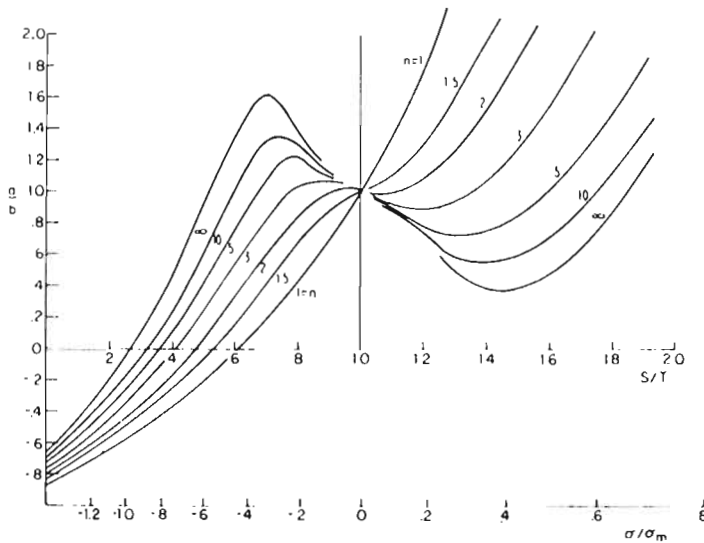

FIG. 5.2. Initial shape change of spherical void.

Void oblateness is obviously significant in void interaction and coalescence under tensile straining, since the cross-sectional area of the void perpendicular to the straining axis is a more important variable in void coalescence than is its volume. A qualitative explanation of the origin of this counter-intuitive effect will now be given.

The deformation of the void in the linearly viscous solid is in accord with geometrical intuition in that one expects a remote tensile strain-rate $\dot{\varepsilon}$ to elongate the void in the direction of straining and detract from growth of its equator. The converse behavior for the void in the nonlinear material under sufficiently high triaxiality is a consequence of two factors—the nonlinear coupling between $\dot{\varepsilon}$ and the spherically symmetric field, and the nature of the flow law (1.3) at high n. Equation (1.3) can be written as

$$\dot{\varepsilon}_{ij} = \tfrac{3}{2} \dot{\varepsilon}_e (s_{ij}/\sigma_e), \quad \text{where} \quad \dot{\varepsilon}_e = \dot{\varepsilon}_0 (\sigma_e/\sigma_0)^n. \tag{5.32}$$

In the rigid–perfectly plastic limit of (5.32), $\sigma_e \equiv \sigma_0$ wherever yield occurs. The spherically symmetric solution ($\sigma = 0$, $\sigma_m > 0$) gives rise to strain-rates given by

$$\dot\varepsilon_r = -\dot\varepsilon_e, \quad \dot\varepsilon_\theta = \dot\varepsilon_\phi = \tfrac{1}{2}\dot\varepsilon_e. \tag{5.33}$$

Imposition of a remote tensile strain-rate $\dot\varepsilon > 0$ induces a large spherically symmetric contribution to the void deformation when $\sigma_m \gg \sigma > 0$ at high n, as has already been discussed. Thus the stresses at the void are determined largely by the spherically symmetric term at high n when triaxiality is high and, from (5.32), this means that the strain-rates are still given approximately by (5.33) at the void. But imposition of a positive $\dot\varepsilon$ gives rise to a variation of $\dot\varepsilon_e$ at the cavity which is largest near the equator and falls to a lower value at the poles. (This observation, which is in accord with intuition, holds for all n, including the linear material.) It follows from this variation and from (5.33) that at high n the void equator lengthens more rapidly than the meridians, i.e.

$$2\int_0^\pi \dot\varepsilon_\theta(a, \theta)a\, d\theta < 2\pi a \dot\varepsilon_\phi(a, \pi/2). \tag{5.34}$$

It is then easy to show that (5.34) implies that $\dot a < \dot b$ for all deformation patterns in which the P_2 variation is the dominant nonspherically symmetric contribution at the cavity.

Andersson (1977) noted growth to oblate shapes in his study of a void centered in a finite cylinder of rigid–perfectly plastic material (5.32). The lateral sides of Andersson's cylinder are free of shear traction and are not permitted to move radially. An imposed overall elongation of the cylinder occurs at the expense of a corresponding increase in volume of the void and induces high triaxiality in the cylinder. Andersson took the void to be a sphere at the start of the overall elongation. As the cylinder elongates the void becomes oblate and grows in this fashion until nearly all the continuing deformation is confined to the remaining ligament between the void and the cylinder surface. The interaction between the void and the cylinder wall is undoubtedly a contributing factor to the development of oblateness in Andersson's void, but it is likely that the effect discussed in the present paper plays the dominant role in the early stages of growth.

6. High-triaxiality Approximation of Growth-rate of Spherical Void

A good approximation to $\dot V$ when $|\sigma_m/\sigma|$ is larger than about unity can be obtained by neglecting all but the spherically symmetric contribution to the velocity $\mathbf{v}$ in the minimization procedure discussed in Section 5. The end result, after some further approximation, is a simple formula for the dilatation-rate of the spherical void. The analysis generalizes a similar one for the rigid–perfectly plastic case given by Rice and Tracey (1969), and the formula derived for $(\dot V/\dot\varepsilon V)$ agrees with their results in the limit $n \to \infty$.

With only the radially symmetric contributions

$$\dot v_r = Ar^{-2}, \quad \dot\varepsilon_r = -2\dot\varepsilon_\theta = -2\dot\varepsilon_\phi = -2Ar^{-3}, \tag{6.1}$$

used in the calculation of Φ in (5.24), we find directly

$$\Phi = 2\pi \int_0^\pi \sin\theta\, d\theta \int_a^\infty \left\{ (3\eta)^{1/n} \left(\frac{n}{n+1}\right)[\dot\varepsilon^2 - \dot\varepsilon Ah(\theta)r^{-3} + 4A^2 r^{-6}]^{(n+1)/2n} \right.$$

$$\left. - (3\eta)^{1/n}\left(\frac{n}{n+1}\right)|\dot\varepsilon|^{(n+1)/n} - \sigma Ah(\theta)r^{-3} \right\} r^2\, dr - 4\pi\sigma_m Aa^3 \tag{6.2}$$

in terms of A and $\dot{\varepsilon}$, with $\sigma = S - T = (3\eta)^{1/n}|\dot{\varepsilon}|^{(1-n)/n}\dot{\varepsilon}$, $\sigma_m = (S + 2T)/3$ and $h(\theta) = 1 + 3\cos 2\theta$.

Introduction of the key variable

$$\Lambda = \frac{\dot{V}}{\dot{\varepsilon}V} = \frac{3A}{\dot{\varepsilon}a^3} \tag{6.3}$$

and the substitution $z = \frac{2}{3}|\Lambda|(a/r)^3$ reduces (6.2) to $\Phi = (4\pi a^3/3)(n/(n+1))(\sigma\dot{\varepsilon})F$, with

$$F = \frac{|\Lambda|}{3}\int_0^\pi \sin\theta\, d\theta \int_0^{\frac{2}{3}|\Lambda|}\left\{\left[1 - \frac{mzh}{2} + z^2\right]^{(n+1)/2n} - 1 + \left(\frac{n+1}{4n}\right)mzh\right\}\frac{dz}{z^2} - \left(\frac{n+1}{n}\right)\frac{\Lambda\sigma_m}{\sigma}, \tag{6.4}$$

where $m = \text{sign}(\Lambda)$.

The quantity Λ may replace A as the single free variable in the minimization of Φ, and so $dF/d\Lambda = 0$ gives

$$\frac{m}{3}\int_0^\pi \sin\theta\, d\theta \int_0^{\frac{2}{3}|\Lambda|}\left\{\left[1 - \frac{mzh}{2} + z^2\right]^{(n+1)/2n} - 1 + \left(\frac{n+1}{4n}\right)mzh\right\}\frac{dz}{z^2}$$

$$+ \frac{m}{2|\Lambda|}\int_0^\pi \left\{1 - \frac{m|\Lambda|h}{3} + \frac{4}{9}|\Lambda|^2\right\}^{(n+1)/2n}\sin\theta\, d\theta - \frac{m}{|\Lambda|} = \left(\frac{n+1}{n}\right)\left(\frac{\sigma_m}{\sigma}\right). \tag{6.5}$$

This can be used, via numerical integration, to provide the desired estimate of the relation between σ_m/σ and $\dot{V}/(\dot{\varepsilon}V)$. However, we can obtain a useful analytical approximation to this result. It is seen that for large $|\Lambda|$ the dominant contribution of the integrals in (6.5) is

$$\frac{2m}{3}(n+1)\left|\frac{2\Lambda}{3}\right|^{1/n}. \tag{6.6}$$

This implies that $m \equiv \text{sign}(\Lambda) = \text{sign}(\sigma_m/\sigma)$ for sufficiently small $|\sigma|$, and also provides the asymptotic approximation

$$\Lambda = \frac{3m}{2}\left|\frac{3\sigma_m}{2n}\right|^n. \tag{6.7}$$

Except for $n = 1$, where it is exact, this estimate for $\dot{V}/(\dot{\varepsilon}V)$ is too crude since it is invalid for $n = \infty$ and has a very small range of validity for large n. The next term in the asymptotic expansion of the left-hand side of (6.5) for large Λ is a constant which is of magnitude comparable to (6.6) as $n \to \infty$ and must be included if an estimate of Λ that is uniformly valid for all n is to be obtained.

To get this better estimate, we write the left-hand side of (6.5) as

$$\frac{2m}{3}(n+1)\left[\left|\frac{2\Lambda}{3}\right|^{1/n} + G(n, m) + \ldots\right], \tag{6.8}$$

where, by subtracting (6.6) from (6.5), we can get

$$G(n, m) = -1 + \frac{1}{2(n+1)}\int_0^\pi \sin\theta\, d\theta \int_0^1 \left\{\left[1 - \frac{mzh}{2} + z^2\right]^{(n+1)/2n} - 1 + \left(\frac{n+1}{4n}\right)mzh\right\}\frac{dz}{z^2}$$

$$+ \frac{1}{2(n+1)}\int_0^\pi \sin\theta\, d\theta \int_1^\infty \left\{\left[1 - \frac{mzh}{2} + z^2\right]^{(n+1)/2n} - z^{(n+1)/n}\right\}\frac{dz}{z^2}. \tag{6.9}$$

The terms omitted in (6.8) vanish for large $|\Lambda|$. The improved estimate for Λ becomes

$$\frac{\dot{V}}{\dot{\varepsilon}V} = \frac{3m}{2}\left\{ \frac{3}{2n}\left|\frac{\sigma_m}{\sigma}\right| - G(m, n)\right\}^n \tag{6.10}$$

and this is a uniformly valid asymptotic approximation, for large $\dot{V}/(\dot{\varepsilon}V)$, for all n.

The formula still requires numerical evaluation of the integrals in (6.9), but now we expand $G(n, m)$ into

$$G(n, m) = -\left[1 + \frac{g(m) - 1}{n} + \dots \right] \tag{6.11}$$

for large n; then

$$g(m) = \lim_{\varepsilon \to 0}\left[\ln \varepsilon - \tfrac{1}{2}\int_0^\pi \sin\theta\, d\theta \int_\varepsilon^\infty \left\{\left[1 - \frac{mzh}{2} + z^2 \right] - 1 - z\right\}\frac{dz}{z^2} \right], \tag{6.12}$$

which can be evaluated analytically to give

$$g(1) \quad = \ln 3 - \frac{2}{3} \cong 0.4319, \tag{6.13}$$

$$g(-1) = \frac{2\pi}{9\sqrt{3}} \cong 0.4031.$$

Finally, we use the approximation

$$-G(n, m) \cong \frac{(n - 1)\left[n + g(m) \right]}{n^2}, \tag{6.14}$$

which is correct to order $1/n$ at $n = \infty$, and correctly vanishes at $n = 1$. A comparison between this approximation to $G(n, m)$ and the numerical evaluation of $G(n, m)$ in (6.9) is shown in Fig. 6.1 for $m = 1$; the comparison for $m = -1$ is equally good. Used in (6.10), this gives our final approximate formula

$$\frac{\dot{V}}{\dot{\varepsilon}V} = \frac{3m}{2}\left\{ \frac{3}{2n}\left|\frac{\sigma_m}{\sigma}\right| + \frac{(n - 1)\left[n + g(m) \right]}{n^2} \right\}^n. \tag{6.15}$$

In the limit $n \to \infty$,

$$\frac{\dot{V}}{\dot{\varepsilon}V} = \frac{3m}{2}\exp\left[g(m) - 1 \right]\exp\left[\frac{3}{2}\left|\frac{\sigma_m}{\sigma}\right| \right]$$

$$= 0.850\exp\left[\frac{3}{2}\left|\frac{\sigma_m}{\sigma}\right| \right] \quad \text{for} \quad \frac{\sigma_m}{\sigma} > 0,$$

$$= -0.826\exp\left[\frac{3}{2}\left|\frac{\sigma_m}{\sigma}\right| \right] \quad \text{for} \quad \frac{\sigma_m}{\sigma} < 0, \tag{6.16}$$

in agreement with the high triaxiality formulas derived by Rice and Tracey (1969).

A comparison of (6.15) with the unapproximated high triaxiality relation (6.5) is made in Fig. 6.2, where the ratio of the two estimates of $\dot{V}/(\dot{\varepsilon}V)$ is plotted against $|\sigma/\sigma_m|$ for various n-values for $m = 1$. Results from (6.5) were obtained by numerical integration. The comparison for $n = 1$ is not shown since both results are exact in this case. The simple formula (6.15) is
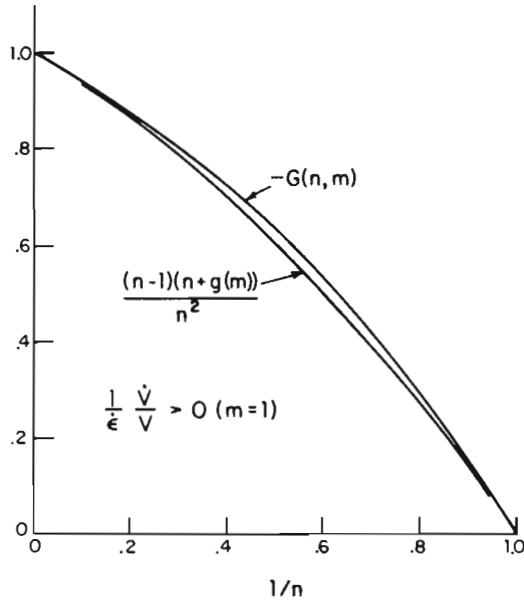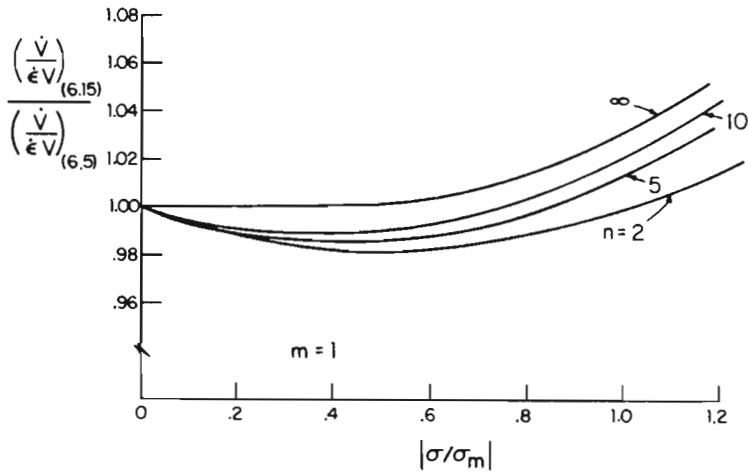
FIG. 6.1. Accuracy of approximation to $G(n, m)$.

FIG. 6.2. Accuracy of analytic approximation for dilatation-rate in high triaxiality range.

within 2 % of the unapproximated result (6.5) for $|\sigma/\sigma_m| < 1$, which is the range of applicability of the high triaxiality approximation. Similar claims hold for the case $m = -1$. Results from the simple formula (6.15) are shown as dashed line curves in Fig. 5.1(b), where they are compared to the predictions obtained from the more extensive calculations of Section 5. For $\sigma_m/\sigma > 2$, (6.15) clearly provides an excellent approximation; and even for σ_m/σ as small as unity, (6.15) underestimates the more accurate results by no more than 20 %.

Multiplying (6.15) by $\eta\dot{\varepsilon} = \text{sign}(\sigma)|\sigma|^n/3$ gives

$$\eta\frac{\dot{V}}{V} = \tfrac{1}{2}\text{sign}(\sigma_m)\left\{\frac{3}{2n}|\sigma_m| + \frac{(n-1)[n+g(m)]}{n^2}|\sigma|\right\}^n \tag{6.17}$$

and it is seen that (6.17) agrees with the spherically symmetric result (5.15) (with $\rho = 0$) when $\sigma = 0$. The strongly nonlinear character of the interaction between σ and σ_m in the high triaxiality range can be seen by comparing the dilatation-rate from (6.17) with the corresponding rate from (5.15) for remote hydrostatic tension or with the rate under remote uniaxial tension from Fig. 5.1(a). As an illustration, for $n = 5$ the dilatation-rate $\dot{V}/V$ of a spherical void under combined σ_m and σ with $\sigma_m/\sigma = 2$ is almost 100 times as great as the dilatation-rate of a void under a pure hydrostatic tension σ_m and more than 10 times as great as that of a void under uniaxial tension σ.

7. Strain to Void Coalescence from Asymptotic Growth-rates $(S > T > 0)$

In this final Section we shall produce a rough estimate of the strain needed to enlarge the voids in a porous solid to the point where coalescence is imminent, following an approach similar to McClintock's (1968) analysis based on cylindrical void solutions. We shall make use of the growth-rate of the asymptotic voids for this purpose since this greatly simplifies the calculations. In Section 3 it was seen that the growth-rate of a void of initially spherical shape in the linearly viscous solid closely approaches the asymptotic value after only a doubling of the initial volume. It seems reasonable to expect similar behavior of voids in the nonlinear materials as well. Of course, if it is assumed that the initial void shape *is* the asymptotic shape then the asymptotic growth-rate truly holds from the start.

Asymptotic growth-rates from the previous Sections are assembled in Fig. 7.1, where we have plotted $(\dot{V}/\dot{\varepsilon}V)_f^{-1}$ as a function of S/T for various n ranging from 1 to ∞. For $1 \leqslant (\dot{V}/\dot{\varepsilon}V)_f \leqslant 3$ the asymptotic shape is a cylinder and the curves in this portion of Fig. 7.1 are obtained from (4.12) and (4.14). (The extensions of these curves into the range $(\dot{V}/\dot{\varepsilon}V)_f < 1$, where the asymptotic shapes are needles, are also given by (4.12) and (4.14).) For $(\dot{V}/\dot{\varepsilon}V)_f > 3$ the asymptotic shapes are prolate spheroids for $n = 1$ and either prolate or oblate pseudo-spheroids for $n > 1$. The curve for $n = 1$ in Fig. 7.1 in the range of asymptotic spheroids derives from (3.6) giving the same relation as (2.28) for the spherical void.

For $n > 1$ only limited information related to the growth-rate of the asymptotic pseudo-spheroids is available; nevertheless, it is sufficient to fill in the dashed-curve estimates in Fig. 7.1. In the high triaxiality range, where S/T is near unity, the growth of the void is dominated by the spherically symmetric contribution and the asymptotic shape will be nearly spherical, although slightly oblate for $n > 1$. The growth-rate for the spherical void should provide a good approximation to the asymptotic growth-rate in this range, and (6.15) has been used to plot the curves in Fig. 7.1 near $S/T = 1$. For increasing S/T the oblateness of the asymptotic shape first increases and then decreases to zero $(a = b)$. For still larger S/T the asymptotic shape is increasingly prolate until it becomes cylindrical at $(\dot{V}/\dot{\varepsilon}V)_f = 3$. The results for the shape change of the spherical void in Fig. 5.2 can be used to estimate the transition of the asymptotic void from an oblate to a prolate shape. We assume that, when $\dot{a}/\dot{b} = 1$ for the sphere, the asymptotic shape will be a pseudo-spheroid with $a = b$ (approximately) and that the growth-rate for the sphere should be a good approximation to the asymptotic growth-rate associated with this transitional shape. The circles in Fig. 7.1 are estimates of these
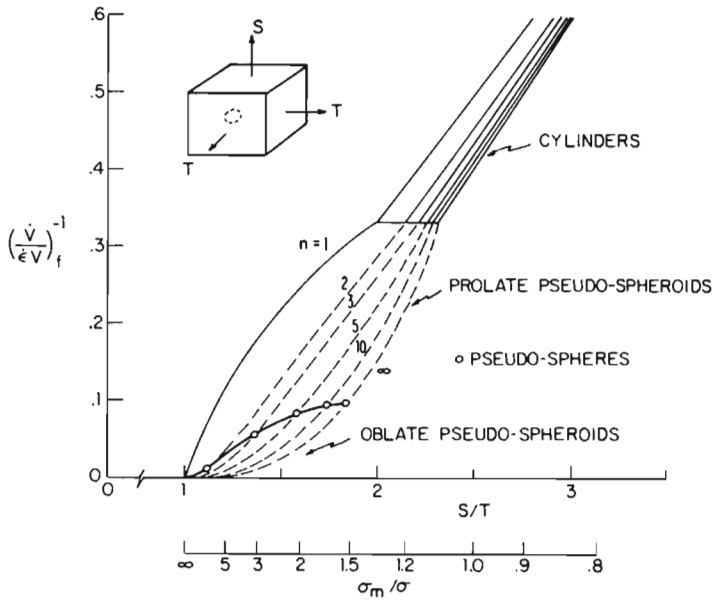
FIG. 7.1. Asymptotic dilatation rates; analytic (solid lines) and estimated (dashed lines).

transitional points so obtained. The remainder of the dashed curve for each n is faired in to connect smoothly the high triaxiality results, the transition point, and the cylindrical limit of the prolate shapes at $(\dot{V}/\dot{\varepsilon}V)_f = 3$. (Subsequent work addressing the accurate calculation of the asymptotic void shapes and their associated growth-rates, published in the *Proceedings of the 15th Congress of Theoretical and Applied Mechanics at Toronto*, reveals that the estimates in Fig. 7.1 are quite reasonable.)

Now we can turn to the problem of estimating the strain at which voids coalesce in a porous block subject to overall stresses S and T in (1.5) with $S > T > 0$. We neglect interaction between the voids and treat each void as if it is isolated in an infinite block, but we relate the growing equatorial radius b of the void in the plane perpendicular to the straining direction to the shrinking distance w between voids in the same plane. Coalescence becomes imminent when b/w grows to some sufficiently large value, $(b/w)_{cr}$.

Whether the shape is a pseudo-spheroid, a cylinder, or a needle,

$$\psi = \dot{b}/(\dot{\varepsilon}b) \tag{7.1}$$

is constant for an asymptotic void growing under fixed S/T. With $b = b_0$ as the initial equatorial radius of the void at the start of straining, (7.1) gives

$$b/b_0 = \exp(\psi\varepsilon). \tag{7.2}$$

The spacing between the voids in the plane normal to S contracts according to

$$\dot{w}/w = -\dot{\varepsilon}/2, \tag{7.3}$$

so that, if w_0 is the initial spacing,

$$w/w_0 = -\exp(\varepsilon/2). \tag{7.4}$$

From (7.2) and (7.4) the ratio of void radius to void spacing increases with strain as

$$\frac{(b/w)}{(b/w)_0} = \exp\left[\left(\frac{1}{2} + \psi\right)\varepsilon\right]$$

(7.5)

and thus the critical strain at which $(b/w)_{cr}$ is attained is given by

$$\varepsilon_{cr} = \frac{2}{1 + 2\psi}\ln\left[\frac{(b/w)_{cr}}{(b/w)_0}\right].$$

(7.6)

When the asymptotic shape is a cylinder or a needle, (4.19) gives

$$\psi = \frac{1}{2}\left[\left(\frac{\dot{V}}{\varepsilon V}\right)_f - 1\right]$$

(7.7)

and thus, from (7.6),

$$\frac{\varepsilon_{cr}}{c} = \left(\frac{\dot{V}}{\varepsilon V}\right)_f^{-1} \quad \text{for} \quad \left(\frac{\dot{V}}{\varepsilon V}\right)_f \leqslant 3,$$

(7.8)

where

$$c = \ln\left[\frac{(b/w)_{cr}}{(b/w)_0}\right]^2.$$

(7.9)

Asymptotic spheroids or pseudo-spheroids satisfy

$$\psi = \frac{1}{3}\left(\frac{\dot{V}}{\varepsilon V}\right)_f$$

(7.10)

whence

$$\frac{\varepsilon_{cr}}{c} = 1 \Bigg/ \left[1 + \frac{2}{3}\left(\frac{\dot{V}}{\varepsilon V}\right)_f\right] \quad \text{for} \quad \left(\frac{\dot{V}}{\varepsilon V}\right)_f \geqslant 3,$$

(7.11)

which equals (7.8) when $(\dot{V}/\varepsilon V)_f = 3$. Curves of σ_m/σ as a function of ε_{cr}/c in the range in which the asymptotic voids are cylinders or needles are shown in Fig. 7.2(a) and are obtained from (7.8) and (4.12). Similar curves on an expanded scale for ε_{cr}/c are shown in Fig. 7.2(b) for the range in which the asymptote voids are pseudo-spheroids. (McClintock's 1968 results for cylinders are essentially equivalent to those in Fig. 7.2(a) but he extrapolates them into the pseudo-spheroid range of Fig. 7.2(b).) The curve for $n = 1$ is obtained from (7.11) and the exact result for $(V/\varepsilon V)_f$ from (3.6), while the curves for $n > 1$ are obtained from the estimates of $(V/\varepsilon V)_f$ in Fig. 7.1.

Interaction between voids is likely to accelerate the growth of the voids and, therefore, to reduce the strain to coalescence below what has been predicted here. Steps to analyze interaction have been taken by Tracey (1971), who models interaction effects for cylindrical voids using a thick cylindrical shell configuration, and by Andersson (1977) with his void in a cylindrical cell which was discussed earlier. More elaborate finite element calculations for planar arrays of voids in plane strain have been carried out by Burke and Nix (1979), Needleman (1972), and Nemat-Nasser and Taya (1976). While it is clear that interaction effects are important in the coalescence phenomenon, it is less clear at what stage (i.e. at what b/w) it becomes essential to allow for interaction. It may be that simple results such as those in Figs. 7.2(a) and (b) which ignore interaction have approximate validity if a judicious choice
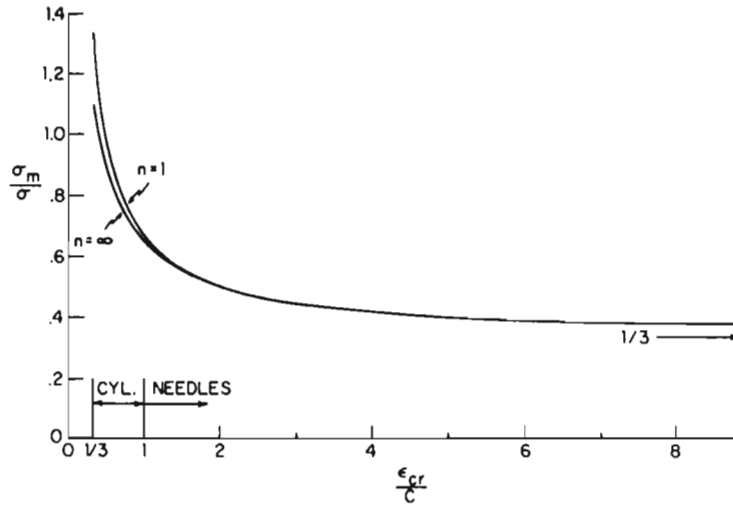
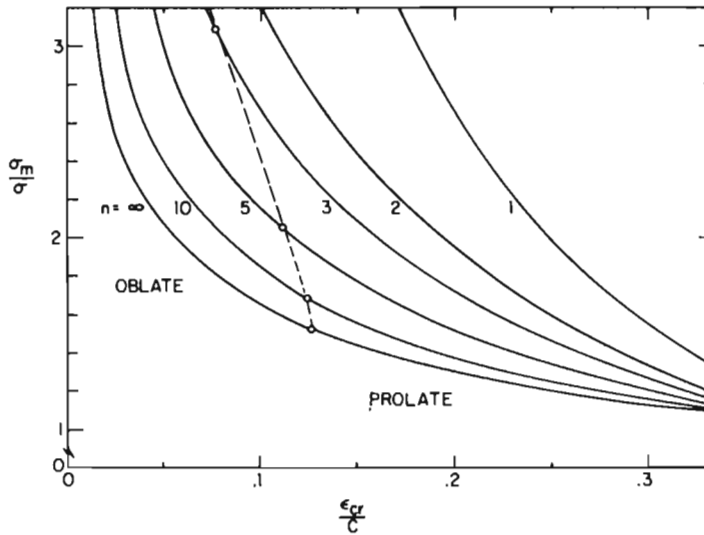FIG. 7.2(a). Critical strain for void coalescence, low triaxiality range.

FIG. 7.2(b). Critical strain for void coalescence, moderate to high triaxially range.

of $(b/w)_{cr}$ is made with the aid of more accurate calculations or with experimental data. Hancock and Mackenzie (1976) and Mackenzie et al. (1977) have carried out a major study of the effect of triaxiality on the ductile fracture of several structural steels. They obtained experimental data in the form of σ_m/σ against ε_{cr} for σ_m/σ in the range 1/3 to 1.4, and they compared their data with curves similar to those in Fig. 7.2(a) based on McClintock's (1968) analysis. While the qualitative trend of σ_m/σ against ε_{cr} was found to be correct, the value of $(b/w)_{cr}/(b/w)_0$ needed to bring the theoretical curve into juxtaposition with the data was

usually unrealistically small. We find similar difficulties in making a quantitative correlation with their data. In the range of low σ_m/σ, where the asymptotic voids are needles (i.e. for $\varepsilon_{cr}/c > 1$ in Fig. 7.2(a)), the predictions for ε_{cr}/c might be expected to err significantly on the high side, since the growth-rate of a void starting out as a sphere is considerably larger than asymptotic rates for needles.

It must be emphasized, however, that for finite n the present results apply strictly to a nonlinearly viscous solid and not to a rigid–plastic solid with strain hardening index n, although in the limit $n \to \infty$ the distinction disappears. The work of Tracey (1971) and Hellan (1975) indicates that the growth-rate of a void in a rigid-hardening solid coincides with the rate of a void in the nonlinearly viscous solid at the same n at low remote strain ε and becomes somewhat larger as the remote strain increases. The constitutive law used here also describes secondary, or steady-state, creep and the present predictions for void growth apply directly when the deformation is dominated by secondary creep. Recent work by Edward and Ashby (1979) and Needleman and Rice (1980) has addressed the problem of void growth when diffusion couples with creep to enhance the rate of growth. For overall states of uniaxial tension, when the growth-rate of the void due to secondary creep alone is low, diffusion is found to make a substantial increase in the growth-rate of the void over an important range of the parameters characterizing diffusion and creep in common metals.

Acknowledgements

References

Andersson, H. (1977) Analysis of a model for void growth and coalescence ahead of a moving crack tip, *J. Mech. Phys. Solids* **25**, 217–233.

Berg, C. A. (1962) The motion of cracks in plane viscous deformation, *Proceedings of the Fourth U.S. National Congress of Applied Mechanics, Berkeley, Ca., June 1962*, 885–892, edited by R. M. Rosenberg. ASME.

Burke, M. A. and Nix, W. D. (1979) A numerical analysis of void growth in tension creep, *Int. J. Solids Structures* **15**, 55–71.

Edward, G. H. and Ashby, M. F. (1979) Intergranular fracture during power-law creep, *Acta Metall.* **27**, 1505–1518.

Eshelby, J. D. (1957) The determination of the elastic field of an ellipsoidal inclusion, and related problems, *Proc. R. Soc. Lond.* A **241**, 376–396.

Hancock, J. W. and Mackenzie, A. C. (1976) On the mechanism of ductile failure in high-strength steels subjected to multi-axial stress-states, *J. Mech. Phys. Solids* **24**, 147–169.

Hellan, K. (1975) An approximate study of void expansion by ductility or creep, *Int. J. Mech. Sci.* **17**, 369–374.

Hill, R. (1956) New horizons in the mechanics of solids, *J. Mech. Phys. Solids* **5**, 66–74.

Hill, R. (1965) A self-consistent mechanics of composite materials, *J. Mech. Phys. Solids* **13**, 213–222.

Mackenzie, A. C., Hancock, J. W., and Brown, D. K. (1977) On the influence of state of stress on ductile failure initiation in high strength steels, *Engr. Fracture Mech.* **9**, 167–188.

McClintock, F. A., Kaplan, S. M., and Berg, C. A. (1966) Ductile fracture by hole growth in shear bands, *Int. J. Fracture Mech.* **2**, 614–627.

McClintock, F. A. (1968) A criterion for ductile fracture by growth of holes, *Trans. ASME*, Series E, *J. Appl. Mech.* **35**, 363–371.

Needleman, A. (1972) Void growth in an elastic–plastic medium, *Trans. ASME*, Series E, *J. Appl. Mech.* **39**, 964–969.

Needleman, A. and Rice, J. R. (1980) Plastic creep flow effects in the diffusive cavitation of grain boundaries, *Acta Metall.* **28**, 1315–1332.

Nemat-Nasser, S. and Taya, M. (1976) Model studies of ductile fracture–I Formulation, *J. Franklin Inst.*, special issue *Basis of the Finite Element Method* **302**, 463–472, edited by K. Washizu.

Rice, J. R. and Tracey, D. M. (1969) On the ductile enlargement of voids in triaxial stress fields, *J. Mech. Phys. Solids* **17**, 201–217.

Tracey, D. M. (1971) Strain-hardening and interaction effects on the growth of voids in ductile fracture, *Engr. Fracture Mech.* **3**, 301–316.